Cold Sintering of Ceramics

Taylor M. Beall

Technische Universiteit Delft

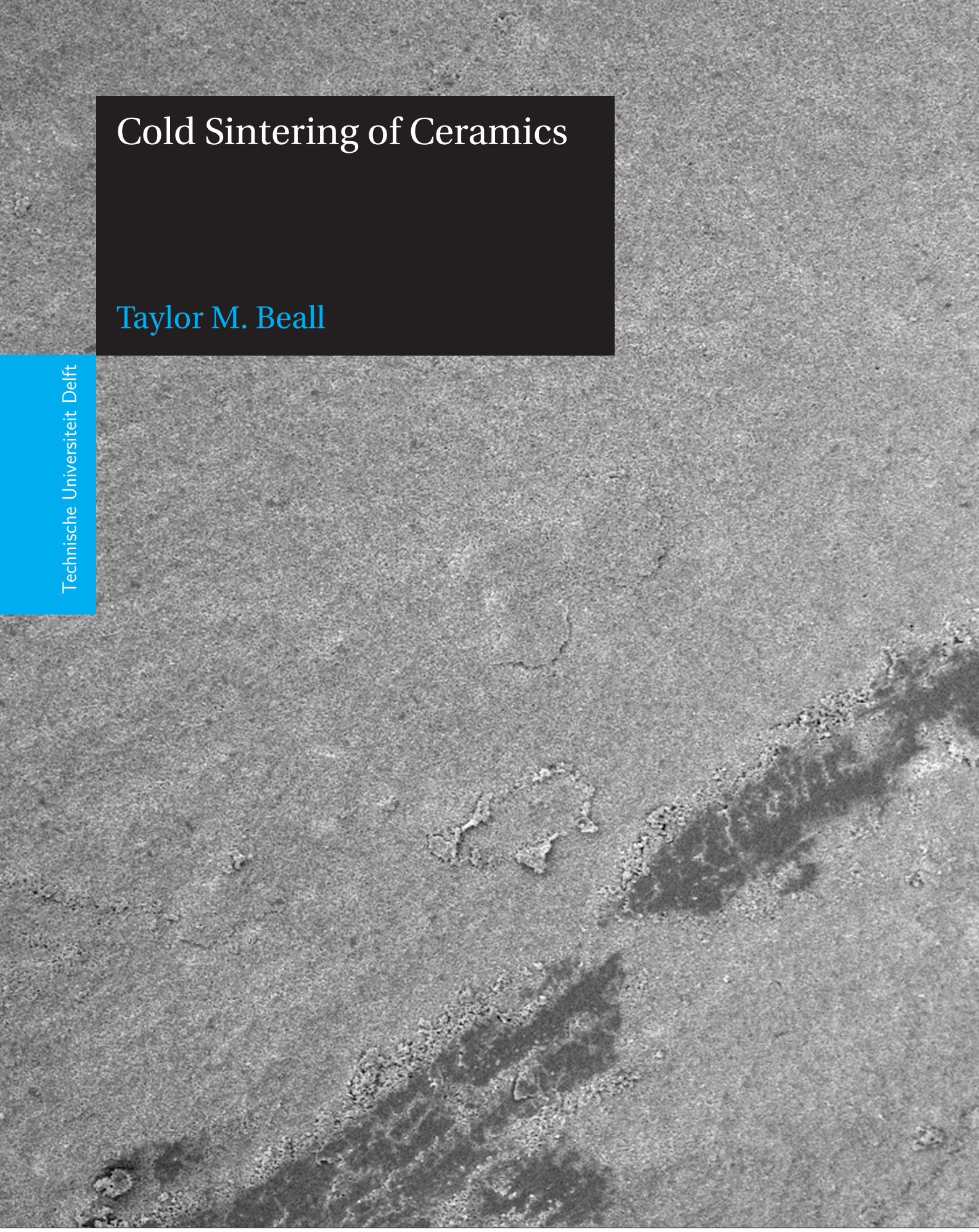

TU Delft Delft University of Technology

Challenge the future

COLD SINTERING OF CERAMICS

by

Taylor M. Beall

in partial fulfillment of the requirements for the degree of

Master of Science
in Aerospace Engineering

at the Delft University of Technology,
to be defended publicly on Tuesday, August 15th, 2017 at 13:00.

Supervisor:	Prof. Dr. W.A. Groen,	TU Delft
Thesis committee:	Dr. J. Bijleveld,	TU Delft
	Dr. J. E. E. Teuwen,	TU Delft

An electronic version of this thesis is available at http://repository.tudelft.nl/.

TU Delft Delft University of Technology

PREFACE

It has been a long road to reach this point, stepping onto the TU Delft campus as a student exactly four years ago. There have been many good times, but unfortunately all good things must come to an end.

My time within NovAM has been really fantastic, and what a fun research group this was! I wish to thank everyone within the NovAM group for their help and guidance over these years. As well, within the lab, I wish to thank all of the talented technicians who helped make this project a success.

In particular, I wish to thank Sybrand for his thoughtful guidance in this project, particularly for steering me toward ideas for tests that helped explain unclear data. As well, I wish to thank Pim, who wisely suggested this topic after I found the first five possible topics not truly interesting enough for me, to work on them for seven months. I am very fortunate to have worked on a project that I am still passionate about.

For the day to day work, I wish to thank Johan, who helped me by converting the tests on paper into reality. As well, his common sense guidance was invaluable. I would also like to thank Daniella who helped me find answers to questions I had, even if it was sometimes in the middle of the parking lot. As well I wish to thank Shanta, who always had ready answers to my multitude of questions.

Beyond NovAM, I wish to thank Gillian and Michiel for their support and help during my time at the TU Delft. Without your encouragement and guidance, I may have never reached the point of this final thesis defense. so thank you.

Finally, I wish to thank my parents who supported me from afar over these last four years. While you probably would prefer that I didn't move further away with each step, I am grateful that you have unquestioningly supported each of my new adventures.

Taylor M. Beall
Delft, August 2017

Contents

LIST OF FIGURES

List of Tables

1

INTRODUCTION

Ceramics serve a critical role in the aerospace industry, particularly in extreme environments where traditional materials often fail. Ceramics can be designed to have an incredibly wide range of properties, leading to uses as diverse as turbine blade coatings, as electrical conductors, and to their perhaps best-known application as Space Shuttle heat shield tiles[1]. Boeing has also been very successful with using piezoelectric ceramics as fuel tank probes, which have the ability to measure fuel amounts accurately at any aircraft orientation [2]. Once formed into the desired shape, ceramic materials require minimal finishing and withstand extreme temperatures that can quickly cause other materials to fail [3]. Beyond their better-known heat tolerance properties, ceramics can also be tailored to have electrical properties[1]. That is where this research thesis attempts to explore.

1.1. CERAMICS

Ceramics have been used for thousands of years, with the earliest evidence stretching back to the upper Paleolithic era [4]. The origin of ceramics starts around 24,000 BC with clay based ceramics as well as glass working. The art of pottery making extended to India and Mesopotamia, and around the world. It took until recent history, however, to start creating the high tech ceramics which are so important to our daily life. High tech ceramics started in the 1800's with the first lightbulb and extend to today, where functional ceramics are frequently used and created in many different diciplines.[5]

The word ceramic derives from the Greek *keramos*. The field of ceramics is broken down into four types of ceramics in two sections. The first section is traditional ceramics, containing the structural, refractories, porcelain and earthenware ceramics. The second section contains technical ceramics.[6] Generally, ceramics start off as powders or clays which are then heated to a point between 50 and 75% of their melting temperature in order to sinter the ceramic with a wanted theoretical density above 95% [4]. These ceramics are polycrystalline, a multitude of small single crystals which are sintered together to make a final solid. This report will focus mainly on the advanced and functional (technical) ceramics[7].

Traditional ceramics are normally manufactured from natural materials such as clays. These materials can be easily found in the Earth's crust and are mainly made up of silicates and aluminum silicates. Due to the wide availibility, low grade ceramic base material can be found almost everywhere, and is one of the main reasons that brick manufacturing is so localized. However, even though the base material for all traditional ceramics is similar,

the process used to create the final product is quite different, especially for finer ceramics, and when glazing is added, even more so. Figure 1.1 shows how traditional ceramics are processed and the various methods used to obtain a final product. Glass is also considered to be a traditional ceramic even though the final product usually looks quite a bit different compared to the final form of clay based material. [8]

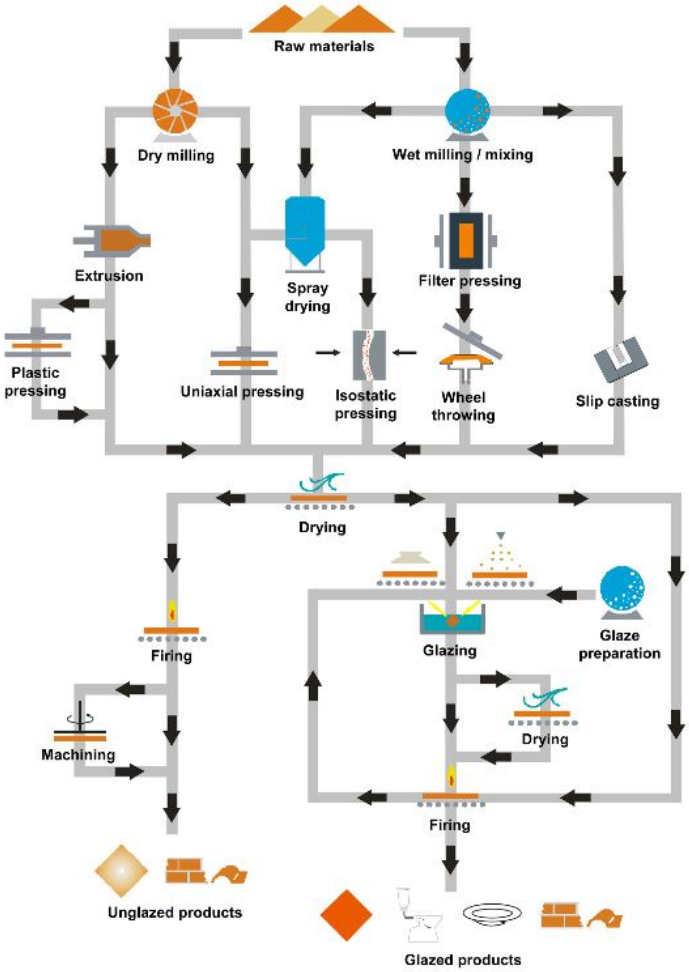

Figure 1.1: Traditional ceramics manufacturing process [6]

As can be seen in Figure 1.1, there are many different paths to the final product in sintering, mainly depending on the raw materials and desired final product. These processes can be more complex, requiring many preprocessing and drying steps before the final firing of the ceramic, or can be very simple, with just mixing and shaping steps needed.

Instead of using clays as raw materials, manufacturing of advanced and functional ceramics is done with high quality powders and strictly controlled processes[7]. The base material might still be the same as for traditional ceramics but simply refined to a higher quality, or it might be a completely manufactured one, created within chemical labs. Beyond the base ceramic properties, these advanced and functional ceramics might have dielectric properties, or other features such as being piezoelectric, allowing for the creation of actuators and sensors.[8]

This thesis will deal with materials in the field of technical ceramics.

1.2. ZINC OXIDE

Zinc oxide (ZnO) is used widely in industry, stretching from the electronics industry to additives to concrete and automotive tires. On top of its use in industry, it is also used in the pharmaceutical and food sectors. [9] This natural material is called zincite, a crystal which is abundantly found in the earth's crust. [10]

There is a difference in properties between the zincite single crystal and the sintered ceramic. As seen in Figure 1.2, the single crystal zinc oxide is completely transparent with a colored tint. This crystal behaves as an insulator. [10, 11]

Figure 1.2: Zinc Oxide Single Crystal [11]

The ceramic form of zinc oxide, which is the format will be used for this thesis, is a dark white to colored material. This material functions as both a conductor and insulator, as will be explained later in this report. [12]

Zinc oxide is used in many different electrical settings, with a melting temperature at 1975 °C [10]. Zinc oxide can be sintered at differing temperatures, allowing for slight changes in the final microstructure and for some tailoring of the final properties. [13] The structure of zinc oxide is normally wurtzite with four oxygen atoms attached to each zinc as shown in Figure 1.3 [14], which is very similar to the zincblende structure of zinc sulfite. Pure zinc oxide is an insulator, while the doped material with group III elements such as aluminum becomes a highly conductive n-type conductor. [15]

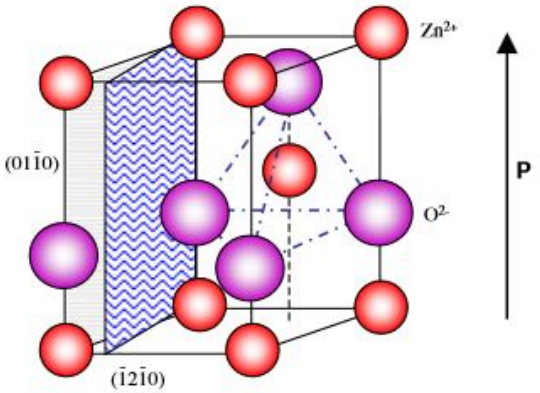

Figure 1.3: Wurtzite unit cell [16]

Zinc oxide is also a prominent piezoelectric material, within the tetrahedral semiconductor group the definite forerunner. This doped material is used often in metal oxide varistors in electronic circuits [9].

1.2.1. VARISTORS

Varistors are similar to resistors in how they function, however, varistors have a very important feature. At low voltages, the varistor has high resistance (acts as an insulator), but as the voltage increases past a certain point, this resistance decreases rapidly [17]. This feature has great use in electronics as a surge protector for sensitive circuits, and do not need to be reset once tripped. Lower voltages cause a linear current-voltage relation, but once the threshold voltage is passed, the power law takes over the relation, with large amounts of current passing through the varistor. Figure 1.4 shows the progression of the current as the voltage is increased [12]. The power law is as follows;

$$I \propto V^{\alpha}$$

where the exponent α shows how rapidly current increases, with values being able to reach around 50. Zinc oxide has the benefit of having a high α value. The major benefit is that this breakdown is reversible, unlike the dielectric breakdown, which is why they are so popular for use of over-voltage protection, as they can offer protection just through applciation in parallel to a sensitive circuit without damage to the varistor or the need to manually reset it. [14]

Zinc oxide is the most commonly used material used for varistors. The intergranular layer within the material allows for electrons to collect on the grain surface, but not be able to tunnel into the next grain until the voltage is high enough. [13] This breakage voltage depends on the physical size of the varistor, particularly the grain size and overall final size, such as a 1 mm thick varistor with 10 μm grains having a breakage voltage of 300 V, or 3 V per grain boundary [14].

Zinc oxide varistors, as well as other metal oxide varistors, are manufactured using a traditional sintering process, which will be discussed later in this paper. Within this process, in order to have a high quality final product, the most critical parts of the process include the powder preparation and the sintering. The initial powder composition is important to make sure that the final product behaves as expected, for the varistor, that there is no premature current leakage. [12]

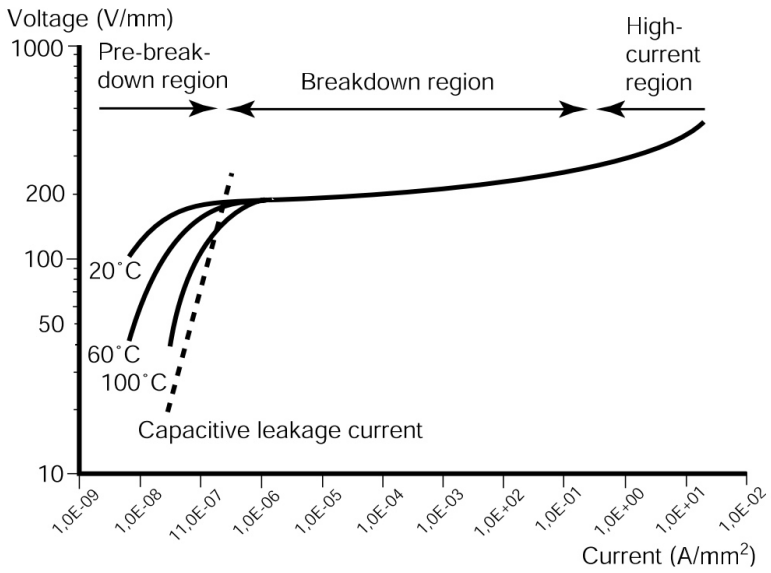

Figure 1.4: Zinc oxide varistor characteristics [12]

These varistors can also have other uses, due to the fact that when the voltage applied to the varistor is above the breakage voltage, the varistor emits visible light. Beyond the use within electronic circuits as a surge protector, this varistor material can be screen printed instead as part of a physical display and used to emit light for the display. [17]

Dopants can also change the properties of the zinc oxide, and since zinc oxide does not require a artifically created microstructure, there is an ease in manufacturing doped material. [17]

The varistors can experience degradation, which is a catastrophic runaway condition. Stabilization of zinc oxide varistors is completed by annealing at 700-800 °C, which makes the varistor less effective at lower voltages, but prevents this degradation from occuring later in life. The application of heat allows for some of the ions to shift to a lower energy state to prevent later applications of energy to have these zinc ions shift to the grain boundaries and lower the resistance.[13]

To further the properties of zinc oxide, the material can be doped. Bechtel et al. [17] worked on doping the varistor layer in a light emitting display. The dopants were one or more of the following materials: Bi_2O_3, Co_2O_3, MnO_2, Sb_2O_3, Al_2O_3, or B_2O_3.

When adding the dopants, usually about 1 mol%, the processing conditions are not changed. Figure 1.5 shows the case for doping with aluminum and mangenese. In this case, Al^{3+} ions end up in the zinc oxide lattice. These ions allow for the creation of electrons from oxygen. Another important dopant is manganese which controls the amount of oxygen vacancies, particularly in the grain boundaries. This prevents the electrons from entering the conductive areas on the exterior of the zinc oxide, which increases the resistance on the exterior of the grains, enhancing the natural properties of zinc oxide and why it is so effective as a varistor material.

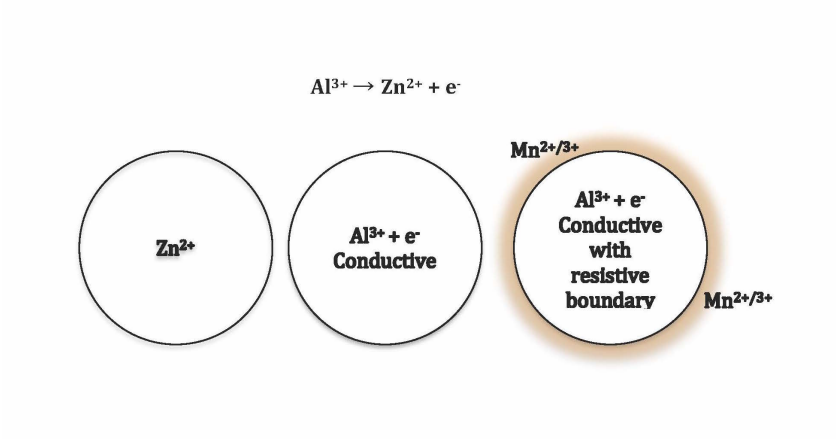

Figure 1.5: Doping process of varistor. Left is pure zinc oxide, middle is the conductive aluminum doped, and to the right is the varistor material where there is mangenese in the boundary

In the case of Bi_2O_3 and Sb_2O_3, these dopants provide a liquid phase which assists in the sintering process. The addition of these two materials also assists in the control of the grain size as well as improving the intergranular contacts between the zinc oxide grains. [13]

1.3. SINTERING

1.3.1. TRADITIONAL SINTERING

There are two main types of traditional processing. The first is to use a fine ceramic powder, mix it with some sort of liquid binder that allows the powder to hold a form, then to shape it into the final shape. This powder-liquid mixture is then fired (or sintered) into one final mass and shape. The second method is the one which is normally used for glass, where the start material is melted to liquid, then formed and cooled back to a solid with a new form. This section will deal with the first of these two processes, the ceramic sintering process.[8]

The raw material used in traditional sintering is an inorganic nonmetallic crystalline solid, which has been formed over time in the surface of the earth. Both the chemical makeup of these raw materials, as well as the crystal form, determine the final properties of the ceramic. The backbone of the ceramics industry uses silicate and aluminum silicate, as they are widely found and inexpensive, and in the case of silicate, have been used for thousands of years. As well as the chemical makeup of the raw material, the quality and purity is also important. For materials such as bricks or other clay items, the purity is less of an issue compared to fine ceramics and technical ceramics. [8]

In order to be able to sinter the raw material into the final form, the raw material must first be prepared. This preparation deals with mainly the particle size of the raw material, as well as the distribution. In many cases, the particle sizes must be very small, in the micron size, however in some cases, two particle sizes will be used. Having a mix of particle sizes allows for a maximum particle packing density to be achieved, the ratio usually around 70% coarse material and 30% fine material. This mix also reduces the warpage and shrinking during the drying and sintering process, as well as helping in the densification process. For the mixing of the material, normally wet mixing is used in a ball mill, plunger, or other device. During the mixing process, shear stress allows for improvement of the mix properties

and distribution of the particles. This wet mix is then dried, and then formed into the final shape for firing. This forming can be done with a dry or wet powder with another added drying step.[8]

The main forming methods include dry or semidry pressing in a mold or processes such as as plastic forming and slip or tape casting. Plastic forming is when the powder is mixed with water or other organic powders to form a material which has plastic behavior. This material is then deformed to the needed shape. Slip or tape casting is when the powder is first created into a slurry, then formed. This final slurry body structure needs to have as few voids as possible to avoid heterogeneous areas within the final ceramic, therefore requiring precise manufacturing. [18]

After the forming step, the final product is then fired, either in a step process to allow for a glazing before the final firing, or in a one step process. Firing is normally used for more complex processes, while sintering refers more to the less complex heating process, such as solid state sintering [18]. Generally, ceramics are sintered at a temperature between 50 and 75% of the melting temperature, preventing the material itself to melt completely but still at temperatures typically higher than 1000 °C [4]. This process for a simple dense ceramic can take from several hours to several days [19]. During this process, there are several main changes. There is a change in the grain size and shape, as well as changes in the pore size and shape. Before firing, there the porosity might be as high as 60%, and the sintering will ideally remove most or all of the remaining porosity. Why this denisifcation occurs is due to the free energy in the system. The system moves to a low energy state, and the energy which runs the sintering process is the surface free energy. The surface energy is this free energy per unit area of the surface area. The reduction of this surface free energy is done by decreasing the surface area by combining many small particles into larger ones. The free energy increases when an atom from the interior is moved to the surface due to the breakage of bonds during this move. Therefore the equation for the change in free energy for constant pressure and temperature is $\Delta G = \gamma(A_2 - A_1)$ with γ being the surface tension of the particle, and A_1 and A_2 being the surface areas of the particles. The system works towards a low energy, therefore with a dense atomic packing of the particles within the solid. [8]

Another way to assist in the sintering process, which was discussed briefly before is to use a mixture of different grain size powders. Adding a mix of powders, adds another grain surface factor into the calculation, and therefore the Gibbs free energy calculation will also change slightly. Taken from the paper of Guo et al., the following equation shows the Gibbs free energy change when a coarse particle is made into nanoparticles. [20]

$$\Delta G = 2/3\bar{\gamma}\bar{s}$$

Where G is the Gibbs free energy, $\bar{\gamma}$ is the mean free surface energy or interface energy, and $\bar{s}$ is the surface area of a particle. This equation can be used to take into account having both nano- and micro-particles within the system by transforming it into the following equation.

$$\Delta G = 2/3\bar{\gamma}(\bar{s}_{nm} - \bar{s}_{\mu m})$$

Where $\bar{s}_{nm}$ is the molar surface of the nano-particles, and $\bar{s}_{\mu m}$ is the molar surface of the micro particles. Using this equation, or more precisly $\bar{s}_{nm}/\bar{s}_{\mu m}$, it can be seen that having a mix or particles can vastly increase the total surface area gain, in some cases by quite a factor. This mix of particles allows for better crystal growth via the Ostwald ripening process, a process which describes the growth of some crystals at the expense of others. This process occurs due to the reduction in free energy, as the surface areas decrease during growth. Having a mix of powders, thereby having a mix of energy states, creates an overall unstable free energy state, helping via the local energy and stress to have crystal growth. [20]

However, care must be taken to actually cause densification instead of only coarsening of the microstructure, as both will reduce the energy, but having only coarsening is not productive to having a final dense ceramic. Figure 1.6 demonstrates the difference between coarsening and densification. The reason coarsening is not preferred over densification is if the energy is reduced through coarsening, the driving force of a high energy for the sintering will also be less. This results in a highly porous final structure, and low overall density. This issue is known in highly covalent ceramics, or when another powder or substance is added to change the sintering from traditional sintering to liquid phase sintering. This form of sintering will be discussed later. [18]

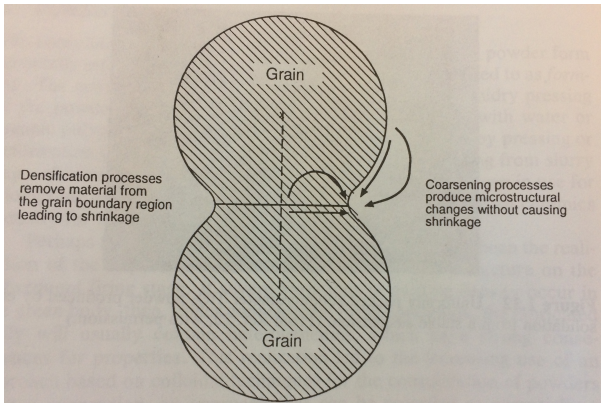

Figure 1.6: Difference in coarsening and densification [18]

As coarsening can occur from two processes, densification or nondensifying processes like surface diffusion, the equation describing this process must contain both of them, as shown in Figure 1.7. This equation can be seen below:
$G^n(t) = G_0^n + \left[B * exp(-(Q_d/kT) + C * exp(-Q_{nd}/kT)\right]t$
Where B and C are constants which depend on the chosen system and k is the Boltzmann constant. Q_d is the energy needed for the densification processes, and Q_{nd} is the energy needed for the nondensification processes. [18]

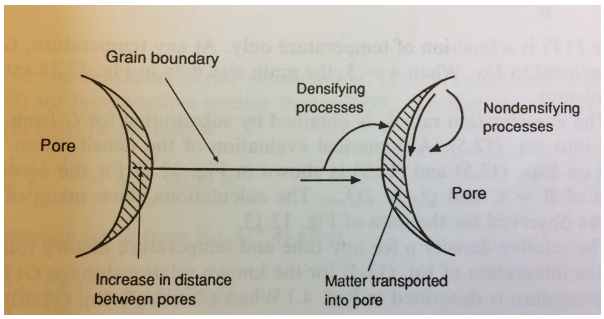

Figure 1.7: Coarsening through densification and nondensifying methods [18]

When constant rate sintering is conducted, the heating rate α can be added to the equation when the equation is integrated over time. Constant rate sintering is slightly different than the isothermal heating, the difference of which can be seen in Figure 1.8. Isothermal heating rates are used more when the system shows high amounts of coarsening at low temperatures. However, the constant heat rate sintering method is closer to what is used in industry with large furnaces which are unable to have as high of heating rates as are required for isothermal sintering.[18]

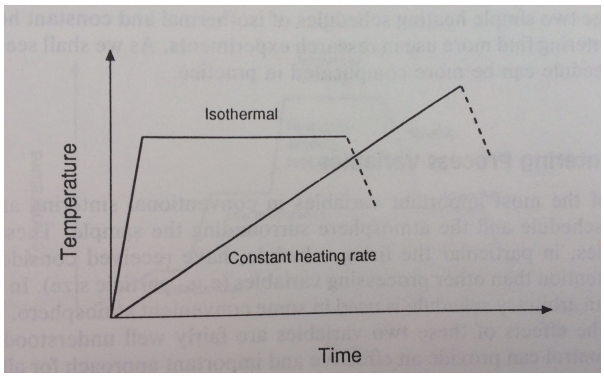

Figure 1.8: Isothermal sintering method versus constant heat rate sintering [18]

As all values besides T are constant for any system, the equation can simplify to the following:
$G^n \approx 1/\alpha * F(T)$
This means that at any temperature the coarsening is inversely proportional to the heating rate, with n usually with a value of 3 for normal zinc oxide sintering. [18]

As well as sintering through the reduction of free energy, there is also mass movement due to the curvature of the particles. The differences of the curvature between the particles as well as the vapor pressure related to this curvature assist in this mass movement. Since this vapor pressure is about an order of magnitude lower at the contact area between particles, it assists in the mass movement within the first stages of sintering, wih the free energy moving the later stages of the sintering process. However, this vapor pressure caused change is restricted mostly to the pores, changing their shape, and requires a high pressure. If pressure is low, then the transfer of material will happen due to solid state processes. This transfer of material occurs from the particle boundary or volume, thereby reducing the radii of the two particles, instead of transfering material from the surface of a particle to the connecting neck to the adjacent particle, which does not increase density of the solid. This is

one of the reasons why the sintering rate is roughly inversely proportional to the particle size, having smaller particles allows for the radii to shrink faster. If the particles are too large, then high densities will not be achieved even if the sintering time is raised. [8]

With regards to temperature, there is what is called 'low temperature sintering', but this process still uses temperature above 1000 °C [21]. When conventional sintering uses terms like low, especially in the terms of cold sintering, they are still relatively high temperatures. The temperature is just lower than the conventional sintering temperature for that material.

1.3.2. LIQUID PHASE SINTERING

Liquid phase sintering is similar to the traditional sintering process, however it, as the name indicates, includes a liquid phase during the sintering process. The starting material is a mix of powders which melt at different temperatures. The powders which melt at lower temperatures create a liquid phase within the material, and typically, the remaining solid grains are soluble in this newly formed liquid, allowing for wetting of the solids and the beneficial capillary force. As the temperature increases further, the remaining solid grains also soften, further aiding in the sintering process. This process is widely used in industry and for many different materials, especially ones which are not possible to create through other methods. [22]

The capillary force is created when the vapor from the liquid phase condenses within the microstructure of the powder. This liquid must be able to wet the solid phases, and the surfaces must be close enough for the bridge to successfully form, which has a negative curvature that draws the two surfaces together. Therefore this force can only work when there is enough condensation, proper wetting, and the solids are close to each other. The final force can be given by:

$$F = 2 * \pi * R_s * \gamma * cos(\theta)$$

where γ is the surface tension, R_s is the grain radius, and θ is the liquid contact angle, in the case of this system with good wetting, less than 90°. [23]

Figure 1.9 shows the microstructre changes over the liquid phase sintering process. Starting with the mixed powders, one melts and allows for assisting of the rearrangement of the solids. As the temperature further increases, coarsening and densification of the material occurs, resulting in the final ceramic material. [22]

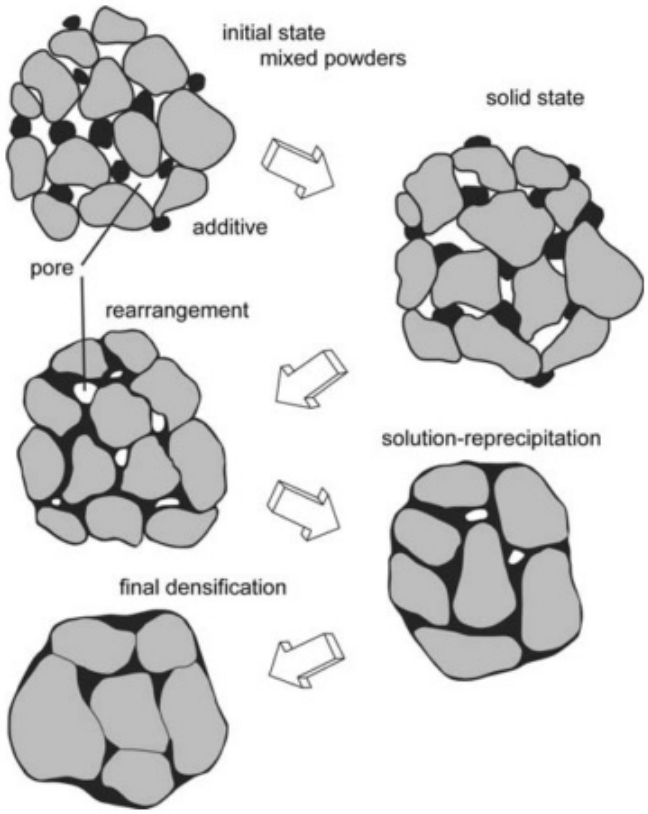

Figure 1.9: Microstructure changes during liquid phase sintering [22]

The addition of the liquid phase can replace large external forces by using capillary forces within the material itself. However, the solubility of the solid grains is important, as having high wetting and a low contact angle allows for ease of transport. If there is a high contact angle and poor wetting, the liquid phase acts more as a pore filler than assisting in the densification process, which can also occur when there is a low liquid content [24]. The liquid content is normally between 5 and 15 vol.% but this can change depending on the system. In rarer systems, the liquid is soluble in the solid, which causes swelling of the material and a final porous structure. [22]

The surface energy is an important aspect in the sintering of the ceramic using this method. Through the liquid wetting the grains of powder and any solubility of the powder, the surface energy of the system increases. This increase in surface energy then increases the grain growth rate and ending densification, as the system progresses to a state of low energy. However, this only works for a good wetting liquid, as if the liquid forms does not wet the particles well, it can actually cause the adverse affect, as the densification of the solid is related to the rate that the solid can transfer through the liquid phase. [25]

This process, while evidence of it exists from centuries ago, has only been truly documented as of 1968. Major advantages of having the liquid phase in the sintering process allows for faster processing of the material into the final form by assisting in the movement of the atoms of the ceramic, along with the capillary action assisting in the same manner as an external force would. However, with every advantage there is a disadvantage. If too

much liquid is formed during the process, it can cause distortion within the final product, something which is not wanted, especially in high tech ceramics. [25]

There are some other drawbacks from this process. One is the large size changes that the material goes through during the sintering process due to the creation of liquid and then later removal of the liquid. This difference in size change between the traditional sintering process and the liquid phase sintering and be seen in Figure 1.10, with the Low-Sintering PZT referring to the liquid phase sintered ceramic. The decrease in the size occurs at a lower temperature, and ends up with a smaller final size compared to the beginning dimensions. The change is also much more drastic, happening in a much shorter time than the traditional processing, due to the addition of the liquid in the process [7]. As well, the liquid phase causes a second phase to end up on the grain boundaries of the final sintered ceramic, though through correct selection of the liquid phase, should not pose to be a problem. [18]

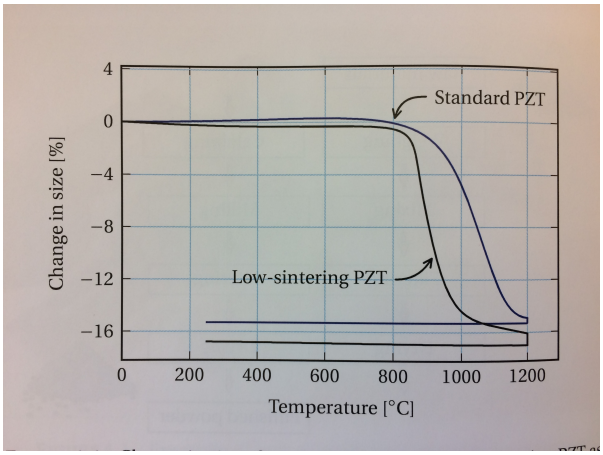

Figure 1.10: Difference in size change during sintering process [7]

The particles also need to be small to aid in the transfer of mass through the liquid phase, and their shape can also affect the end density. The temperature must be over the required liquid temperature, and further increases can aid in the sintering, however then the time must be adjusted accordingly so that there is no problem with the increased temperature. Low soluability ceramics are processed more successfully at higher temperatures. [25]

1.3.3. HYDROTHERMAL SYNTHESIS

Hydrothermal synthesis refers to the synthesis process of normally insoluble materials in a high temperature and pressure environment using aqueous solvents. While there are some inconsistencies in definition between different researchers, there is a general consensus regarding the use of pressure greater than atmospheric pressure, as well as temperatures greater than room temperature. This broad definition should encompass all the various different hydrothermal synthesis processes from different materials. [11] Hydrothermal synthesis is used to assist reactions which would normally not be very successful in normal conditions. Examples of processes include solid reactions, dissolution and recrystallization of some substances, and doping and phase creation. [26]

While the research regarding hydrothermal synthesis stretches back to the 1800's, large scale work was not started until the late 1940's. The research began in Europe and the United States, and then spread during later years into Asia, where some of the world leading research is conducted today, such as Japan being the largest producer of quartz, with the largest autoclaves in the world. [11]

For hydrothermal synthesis, since the system is a closed one, what materials are placed into the system at the beginning have a large effect on the success of the process as well as what the final product is. Beyond that, the temperature will affect the synthesis as well as the pressure. Finally, the amount of time the system is run will also effect the size of the final product.

The solvent choice and parameters is quite crucial to have this synthesis process work as intended, with most initial failures due to poor solvent choice. Along as acting as the physical transfer medium during the synthesis, it also can act as an absorbent, solvent and reactant, 4 important actions. Water is normally a large part of the solvent, allowing for the ability to take advantage of the critical point of water. In the beginning of the research on this topic, only water was used in most experiments. However, while using water was successful, it does not work for every single material process, and the final crystal size was relatively small, in the size of hundredths or thousandths of millimeters. Therefore more advanced solvents are normally used now instead of water. [11] Currently, the addition of a electrolyte material into the solvent is done to assist in the synthesis of chemically inert materials.

Each of the four actions of the solvent chosen has an important effect on the process. Starting with the transfer of the solid state material (1), this is done through erosion or other abrasion of the particles, in essence transferring the kinetic energy of the system. The absorbent aspect of the solvent allows for surface diffusion, crystallization, ion exchange and other sintering movements within the system (2). The solvent action does as it sounds, it dissolves the solid state and precipitates it in other areas, allowing for crystal growth and synthesis (3). Finally the reactant action allows for the hydration of the system, creating oxides and hydroxides (4). Figure 1.11 shows these four actions with examples. [11]

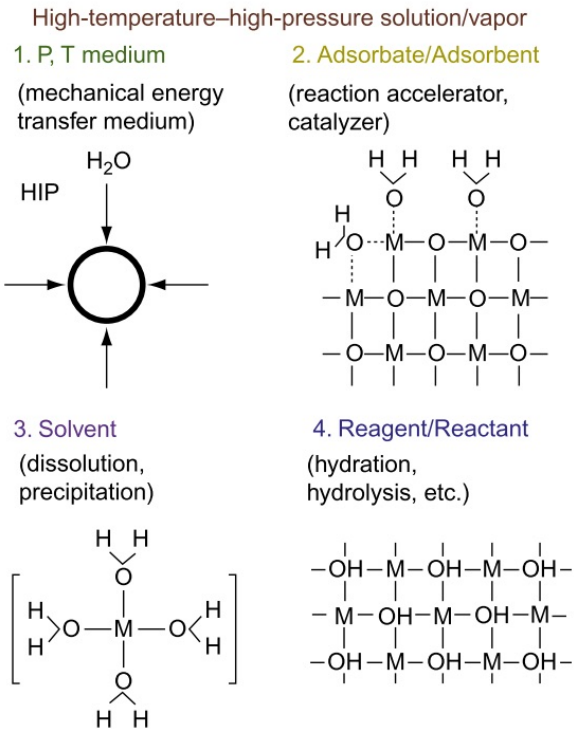

Figure 1.11: Examples of the solvent actions [11]

As well as using a solvent, more and more processes now use a surfactant within the system to separate the solvent and the other material within the system, whether it be air or another solvent. This method is used more for advanced materials to be able to further control the properties of the final product. [11]

1.4. SOLUBILITY

For this thesis, it is expected that the solubility of the powders will be crucial in the success of the process of cold sintering. The soluability of zinc can be seen in Figure 1.12. In acidic environments, the form of zinc shifts to the positive ion. As the pH turns basic, zinc hydroxide is the leading form, and at the highest base levels, negatively charged zinc super oxide is formed. [27]

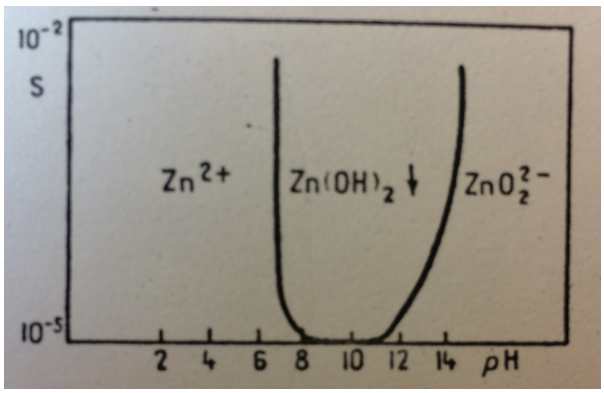

Figure 1.12: Zinc solubility diagram [27]

This shows that in order to dissolve the grains, an acidic solution must be used, or an very basic one, as zinc hydroxide is not soluble and will precipitate out of the solution.

Moving to the dopants, the solubility diagram of aluminum is shown in Figure 1.13. Compared to zinc, aluminum requires a slightly lower pH to allow for dissolution, around 4, while zinc needs a pH just lower of neutral at 7. This indicates that when doped with aluminum, as long as the acidic solvent used has a pH lower than 4, it should suffice for both zinc oxide only ceramics as well as those doped with aluminum.

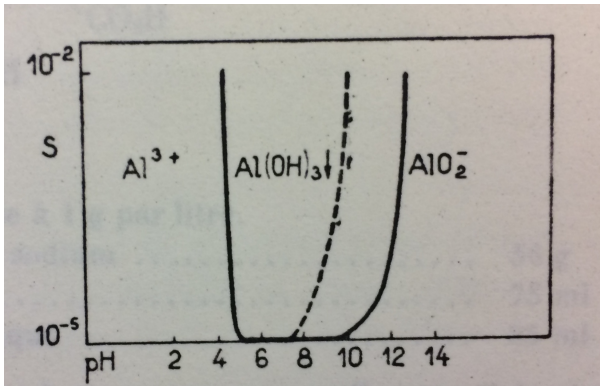

Figure 1.13: Aluminum solubility diagram [27]

As could be expected, many materials have this feature of dissolution in acidic environments, as can be seen in the following Figures 1.14 and 1.15. Mangenese has a similar dissolution pH compared to zinc, with a value around 7, and cobalt also requires an acidic environment to dissolve. This might indicate that it would behave similarly when being prepared for the cold sintering process.

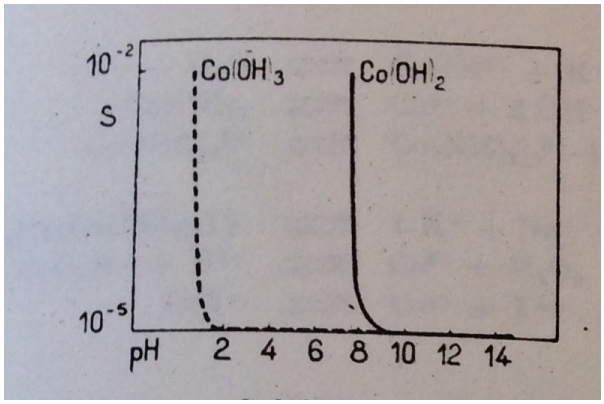

Figure 1.14: Cobalt solubility diagram [27]

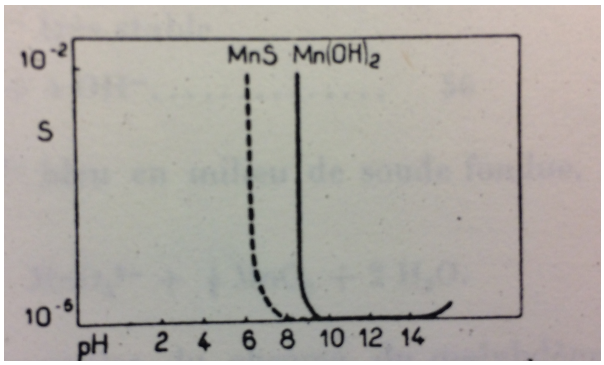

Figure 1.15: Mangenese solubility diagram [27]

So for all materials which will be used as dopants, an acidic solvent is required for dissolution of the grains. As will be explained later in the report, dissolution of the powder grains is a powerful tool in the cold sintering process.

1.5. COLD SINTERING PROCESS

Cold sintering is a process which is quite new, with the bulk of the research having been conducted within the last year by an American group led by Clive Randall at The Pennsylvania State University (PennState). Cold sintering is revolutionary in the way that it simplifies the overall sintering process, drastically reduces the amount of energy required, as well as cutting the processing times from hours to minutes in most cases.[28] There have been a number of other efforts to try and reduce the temperature and make the sintering process more effective, but they mostly then use high electrical energy, thermal steps, or high pressures, and the temperatures are still above 400 °C. [19]

Cold sintering is in essence how the name sounds, that it is sintering of ceramics and other materials at lower than normal temperatures. What this means is that instead of having sintering occur at temperatures greater than 1000 °C, the sintering temperature is lowered to 200 °C and an external pressure is applied during the sintering process. These changes allow for the still successful sintering of the materials by adding a liquid phase to the ceramic powder before the shaping and sintering occurs. This aqueous solution can be water, or more commonly an acidic solution. The solution can also be basic, but so far this is not as common as acidic solutions. This pre-wetting of the ceramic grains allows for dissolution of the edges of the grains, as discussed earlier in this report with the actions of the solvent in the hydrothermal synthesis. The other solvent actions also take place in this process, assisted by the external pressure, to allow for dissolution and rearrangement of the solid through the liquid to cause a surface energy reduction. This process can be seen in Figure 1.16 where the steps from initial powder preparation to final sintered product is illustrated. Finally, the remaining amorphous phase can end up in the remaining pores of the solid. [4]

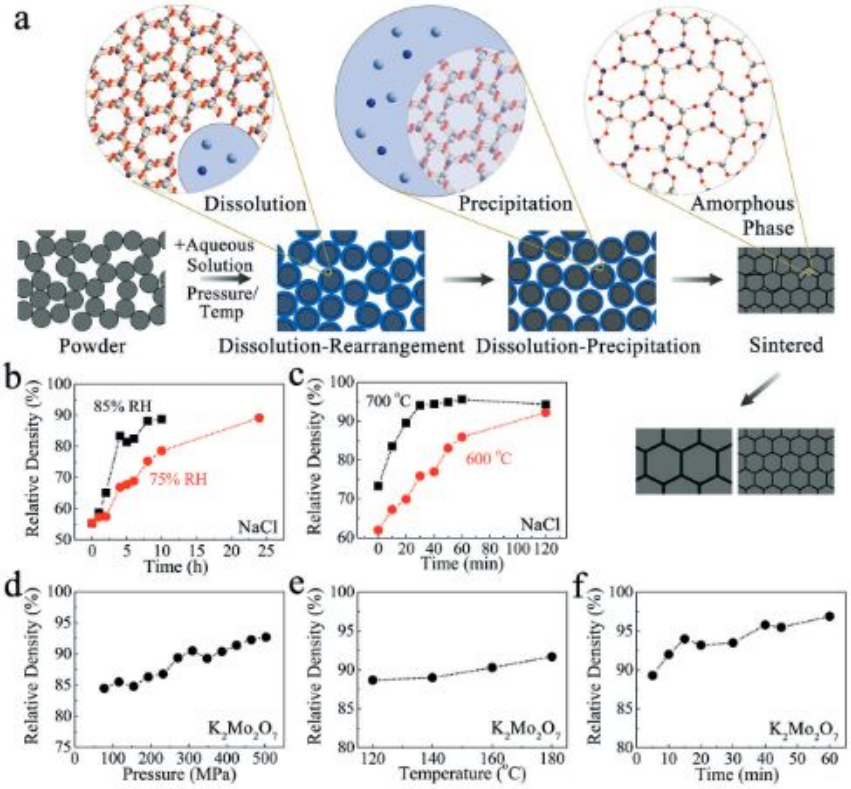

Figure 1.16: a) Demonstration of the cold sintering process from the powder to final sintered product. b) Density of room temperature cold sintered NaCl in various humidity. c) Density versus time of conventionally sintered NaCl. d-f) comparison of density improvement of $K_2Mo_2O_7$ with increasing pressure, temperature and time respectively. [4]

The first literature was published by a research group at the University of Oulu in Finland when they discovered the possibility of cold sintering lithium molybdate, as well as doped versions with titanium oxide or barium titanate at varying volume percentages [29, 30]. They used water as the solvent, though when the insoluble dopants were added, they had some issues with the processing of the material. Possible explanations will be contained later in this chapter when discussing solvent choice. It was found that the resulting final product from this process was very good, and showed the first steps in this field.

1.5.1. PROCESS

Depending on the desired final ceramic, the exact process does vary somewhat, especially the solvent choice and pressure. With the chosen initial powder composition, a small amount of the chosen solvent is then mixed into the powder to create a homogeneous mixture to allow for the surfaces of the solid to dissolve. This mixture is then placed into a chosen mold. This mold must be able to withstand high pressures, as they can go up to around 500 MPa in some cases, and while the pressure is applied, the mold and therefore the powder mixture is heated.

The cold sintering process works as follows. The added liquid to the powder system adds a layer of lubrication between the powder grains. Beyond this lubrication, the solution also removes any of the sharp corner or edges of the grains through dissolution to

further aid in the movement of the grains against each other. This can be seen in Figure 1.17 in stage I. Alongside the lubrication and dissolution, there are three possible processes which assist in the movement within the system and further the densification. Between the solid-solid interfaces within the powder, there is what can be referred to as liquid enhanced creep, which in the diagram is called pressure solution. This is a more advanced and faster version of normal creep due to the addition of a liquid in a solid which takes advantage of the greater solubility between the grains due to a stress difference between the adjacent grains. This has been thoroughly investigated within the field of geology, and explains the mass transport from the grain contacts to the pore space as the liquid flows throughout the system.[19]

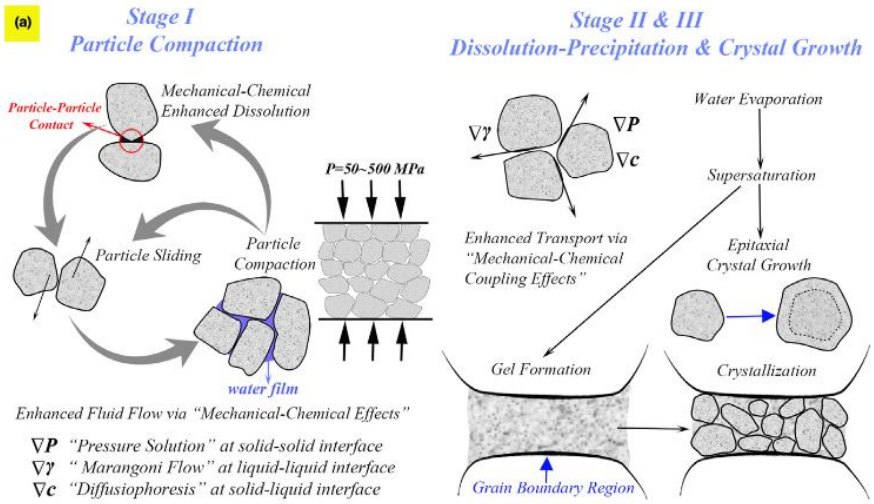

Figure 1.17: Illustration of the specific stages within the cold sintering process[19]

Moving on to the liquid-liquid interface, the Marangoni effect most likely works here. This effect is controlled by the surface tension gradient on the interface, which can be due to the concentration of solute in the solution along the interface, or the temperature. Since there is already dissolution of the solid into the liquid along the solid-solid boundaries, most likely in the cold sintering process it is due to the gradient of the solute concentration within the solvent, and not the temperature. Finally, there is an effect between the solid-liquid interface within the system, and for this interface, diffusiophoresis takes control. Using a slip-velocity at the solid-liquid interface caused by the gradient of the solute concentration, the solid particles can be carried through the system.[19]

After this cold sintering process, if there is any concern that not all liquid has evaporated from the ceramic, the ceramic can then be baked at 200 °C overnight. In some cases, unfortunately, the cold sintering process is not enough to get a dense enough ceramic, therefore an annealing stage is required usually around 700-900 °C to further increase the density to high enough levels. This is especially the case for piezoelectric materials such as barium titanate, the micro-structure can be seen in Figure 1.18. [31]

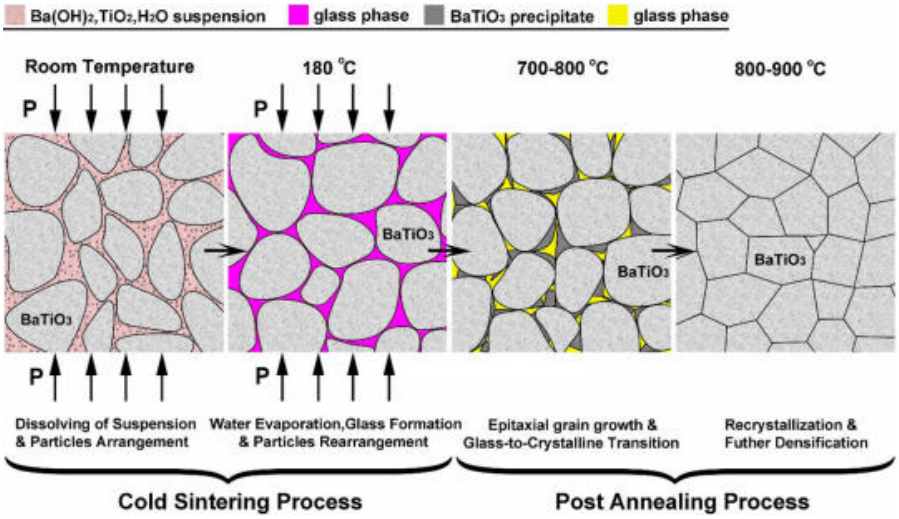

Figure 1.18: Micro-structure of barium titanate from the starting mixture to the final sintered process after annealing [31]

In terms of zinc oxide, Guo et al. was able to demonstrate that it is possible to cold sinter zinc oxide using acetic acid and water as the liquids added to the powder, and they were pressed at various pressures, and sintered at various temperatures. The powder was mixed with 20 wt% 0, 0.1, 1.0, and 17.5 M acetic acid aqueous solution, pressures were either 0, 77, or 387 MPa, and the sintering temperatures were 25, 88, 126, 177, 238, or 305 °C. The timing was taken at 0.25, 1 or 2 hours, and heated at 5 °C per minute and air cooled. [32]

It was found that for the 1 M samples at 126 °C for 1 hour the higher the pressure, in this case up to 387 MPa, the higher density was found in the final product as seen in Figure 1.19. The following figures demonstrate the effect of one variable on the whole.

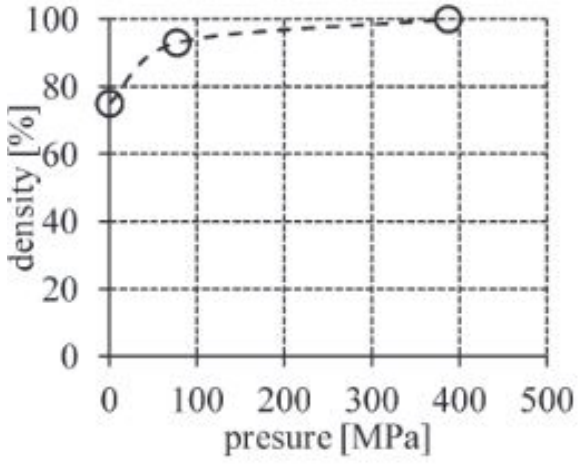

Figure 1.19: Densities of cold sintered zinc oxide versus pressure with 1 M acetic solution[32]

While in this case, the highest density was found with the higher pressures, however, after 100 MPa there was a plateau in the data with the vast majority of the improvements occurring before 100 MPa. For the time, as seen in Figure 1.20, a longer time is better at 126

°C to get a higher density within the final ceramic. Again, there is a plateau at around one hour of processing, with the density perhaps even decreasing at the 4-5 hour range.

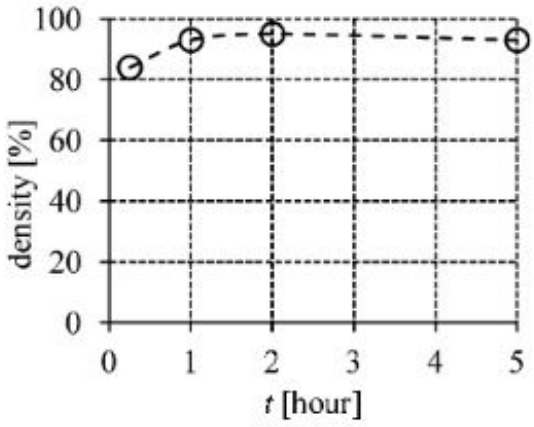

Figure 1.20: Densities of cold sintered zinc oxide versus time with 1 M acetic solution[32]

However, this trend does not hold when looking at just the change in temperature when having a sintering time of one hour. As shown in Figure 1.21, there is a peak within the density when varying temperature are around 100 °C. While the density does increase again at around 300 °C, this temperature puts this specific process outside of the range of the cold sintering. As well, the density at around 100 °C seems to also be higher than this one at 300.

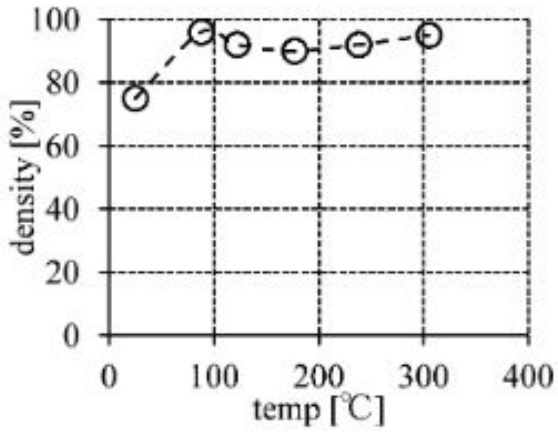

Figure 1.21: Densities of cold sintered zinc oxide versus temperature with 1 M acetic solution[32]

These trends show that for this method there seems to be a peak value for most of the variables, and that outside of this value, or perhaps small range, the density of the final product starts to again decrease. Within the range, the density seems to be consistantly higher than 90 %. However, there Guo et al. did find some issue with the conductivity of the final material, with the material sintered at 126 °C having a conductivity of only 0.00002 S/cm, 305 °C having a conductivity of 9 S/cm, and the conventionally sintered material at 1400 °C having a conductivity of 5 S/cm [32].

1.5.2. PARAMETERS OF COLD SINTERING

The parameters in cold sintering are quite essential to the successful outcome of the final sintered product. This means that quite a number of variables need to be well planned and have everything come together in the end. Figure 1.22 shows a flow chart explaining the different paths which can be taken.

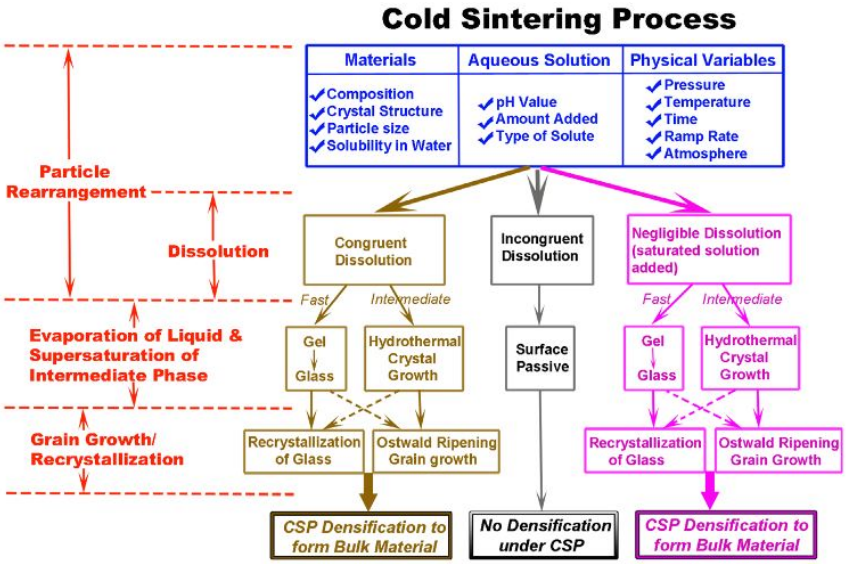

Figure 1.22: Flow chart explaining the different paths to get to a(n) (in)properly created ceramic using cold sintering [19]

As demonstrated within this flow chart, the dissolution is the first step in the process, highlighting the need for proper solvent choice as well as proper powder properties. Of course, further on the rest of the variables come into play, such as the temperature, and pressure applied to the powder.

Initial Powder Properties

For the initial powder properties, in most cases, having a smaller powder size appears to be allow for more consistent, homogenous, and overall better final products when using the cold sintering process. Smaller powder also decreases the size and amount of voids as well, and has better grain attachments. Kähäri et al. found that when using smaller powder, which has a larger surface area, required more solvent in the system for processing to prevent warpage and cracking.[30]

Guo et al. discovered that nanoparticles allow for the most productive cold sintering process as it increases the surface areas. However, it might be the case that it effects the bulk [electrical] properties of the system, something which seems to be able to be overcome with the addition of dopants. [33]

Solvent Type

The solvent used in the cold sintering process is quite important to have a dense and fully sintered final product. This solution provides the correct environment for the chosen ceramic system to provide the same actions as the solution did in the hydrothermal synthesis,

that of mass transport, dissolution, precipitation, and recrystallization. Using a liquid allows for ease of sintering, as the movement of mass is more effective through the solvent than that of solids or melt. Depending on the ceramic type, the choice of solvent is important, such as the pH, concentration of the solvent, type of solute (does it dissolve easily or not)[19].

Kähäri et al. found that they had some more processing difficulties when processing the doped material. In the report from their research, they seemed to rely primarily or only on the properties of lithium molybdate for dissolution and sintering instead of a mix of the properties of both powders[29]. Since the solvent was deionized water, it might be the case that the processing problems was due to the fact that the added dopant powders were insoluble within water, and that perhaps a slightly acidic solvent could improve the process.

Temperature

The temperature choice for the cold sintering process is an important one, even though the overall range is relatively small, spanning from room temperature to 200 °C. The choice of solvent will affect this temperature, as the temperature should be above the boiling point of the solvent, as it allows for both the dissolution as well as a highly dynamic state due to the temperature. [20]

Time

For cold sintering, the time required to complete a sintered product is normally significantly less than for conventional sintering. The cold sintering process usually takes in the range of minutes, usually circa 30 minutes or even less in a number of cases. While an increase of temperature might not allow for a significant increase in density, increasing the time of cold sintering can in fact allow for an increase in the final density, especially when coupled with an increase in pressure. [4, 20, 34, 35]

Pressure

The pressure used in cold sintering can vary, from approximately 50 MPa to 500 MPa depending on the material being sintered[36] in many cases around 250-350 MPa. As the pressure aids in the sintering process, having a lower pressure usually results in a less dense final product, and the density will increase as the pressure increases. With this pressure increase, the time usually must also increase slightly, usually by 10-15 minutes.[4] However, it seems as the exact pressure needed is found through experimental work and calculation of the final density.

1.6. THESIS OBJECTIVE

The main objective of this thesis is to determine if it is possible to manufacture aluminum doped zinc oxide ceramics, using a cold sintering process of using high pressure and less than 200 °C. If this is proven to be possible, then an optimum of the sintering parameters needs to be chosen. This choice will be based primarily on density measurements, as the final ceramic needs to be dense, as well as micro-structure analysis.

As zinc oxide is doped with various other materials to improve its properties, the possibility of doping these cold sintered zinc oxide ceramics will be explored. It is expected that

as long as both materials are soluble in the chosen solvent, that it should be possible to sinter ceramics at similar or the same parameters as was used for the zinc oxide ceramics.

Beyond this, as the solubility of the powder seems to be quite important for this process to be successful, a series of tests using various pH solvents will be conducted. It is expected that as long as the pH is within the soluble range on the zinc solubility diagram, that it will be successful, however, the final properties of the material might not be the same.

For this project, first zinc oxide ceramics will be created to determine if the cold sintering process is possible, then a selection will be made of optimum parameters. From there, these parameters will be used to cold sinter a series of doped samples, where their properties will be determined in relation to the zinc oxide ceramics as well as each other. Finally, some more tests will be conducted to explore pH, and heat treatment (annealing) of the cold sintered ceramics.

2

Material Selection and Experimental Techniques

After a number of iterations, the manufacturing process used to create the samples for this thesis ended up being quite straightforward. This section will clarify what base materials and equipment were used, as well as the explain the final process to create cold sintered ceramics.

2.1. Zinc Oxide Powder

After some deliberation, Zinc Oxide was chosen to be the base material for the cold sintered ceramics. In order to eliminate any possible issue with having too large initial grains, a small grain size of between 40 and 100 nm was used. The material 45849 Zinc oxide, NanoArc ZN-0605 was ordered from Alfa Aesar. The same batch of material was used for all samples in this thesis.

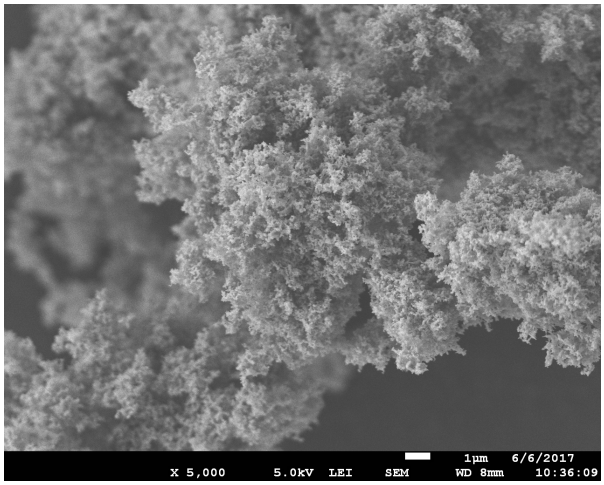

Figure 2.1: Scanning electron microscope imagery of the zinc oxide powder

Due to the small grain size of the powder, as can be seen in Figure 2.1, the powder was extremely light and proper safety measures needed to be taken. Work was conducted in a fume hood, and loose powder was kept in a sealed container until the solvent could be added and the risk of loose powder escaping was minimized.

2.2. SOLVENT

2.2.1. ACETIC ACID

As in the experiments of Funahashi et al. [32], acetic acid (CH_3COOH) was the chosen solvent for the experiments. A solution of 1 molar was diluted from glacial acetic acid (99.7%), and was used for all samples in this thesis.

$$\text{Density} = 1.049 \text{ g/mol}$$
$$\text{Density} = 1.049 \text{ g/mol}$$
$$\text{Molecular Weight} = 60.05 \text{ g/mol}$$
$$(99.7 * 1.049)/60.05 * 10 = 17.416 \text{ mL}$$

In order to create a solution of just 1 mol, the amount of acid required to create 250 mL of the needed molarity was the following.

$$M_1 * V_1 = M_2 * V_2$$
$$17.416 * V_1 = 1 * 250$$
$$V_1 = 14.354 \text{ mL concentrated acid}$$
$$250 - 14.354 = 235.646 \text{ mL water}$$

The pH was also calculated using the pKa listed in literature.

$$[H^+] = (-K_a + \sqrt{K_a^2 + 4 * K_a * C})/2$$
$$\text{pH} = -log[H^+]$$
$$K_a = 1.75 * 10^-5$$
$$\text{C} = 1.0 \text{ mol}$$
$$[H^+] = 4.17 * 10^-3$$
$$\text{pH} = 2.37$$

As this solution is acidic, it is expected to perform as a proper solvent for all samples, pure and doped.

2.2.2. FORMIC ACID

To further explore the effect of pH on the sintering process, formic acid ($HCOOH$) was also used as a solvent. The starting solution was 98 weight% formic acid, which made the original molarity the following.

$$\text{Density} = 1.22 \text{ g/mol}$$
$$\text{Molecular Weight} = 46.03 \text{ g/mol}$$
$$(98 * 1.22)/46.03 * 10 = 25.97 \text{ mol}$$

In order to create a solution of just 1 mol, the amount of acid required to create 0.5 mL of the needed molarity was the following.

$$M_1 * V_1 = M_2 * V_2$$
$$25.97 * V_1 = 1 * 0.5$$
$$V_1 = 0.019 \text{ mL concentrated acid}$$
$$0.5 - 0.0193 = 0.481 \text{ mL water}$$

The water was first measured out and the acid added to it before it was then poured into the powder in the same manner as the premixed acetic acid solution, which will be clarified later in this section.

The calculated pH is as follows:

$$[H^+] = (-K_a + \sqrt{K_a^2 + 4 * K_a * C})/2$$
$$\text{pH} = -log[H^+]$$
$$K_a = 1.77 * 10^-4$$
$$\text{C} = 1.0 \text{ mol}$$
$$[H^+] = 0.0132$$
$$pH = 1.89$$

So the formic acid solution is slightly more acidic than that of the acetic acid solution with the same molarity.

2.2.3. AMMONIA

As well as a second acid, a basic solution as used for a solvent, consisting of 1 molar ammonia solution (NH_3). This was created from a solution of water mixed with a more concentrated 25 wt% solution of ammonia. The initial solution molarity was calculated first:

$$\text{Density} = 0.696 \text{ g/mol}$$
$$\text{Molecular Weight} = 17.031 \text{ g/mol}$$
$$(25 * 0.696)/17.031 * 10 = 10.2 \text{ mol}$$

As the molarity was higher than the required, it was then mixed into water.

$$M_1 * V_1 = M_2 * V_2$$
$$10.2 * V_1 = 1 * 0.5$$
$$V_1 = 0.049 \text{ mL concentrated acid}$$
$$0.5 - 0.049 = 0.0451 \text{ mL water}$$

The pH was also calculated using the pKb.

$$[H^+] = (-K_b + \sqrt{K_b^2 + 4 * K_b * C})/2$$
$$\text{pH} = 14 + log[H^+]$$
$$K_b = 1.75 * 10^-5$$
$$\text{C} = 1.0 \text{ mol}$$
$$[H^+] = 4.17 * 10^-3$$
$$\text{pH} = 11.62$$

Since the pH is above 7, the solution is considered to be basic.

2.3. SINTERING PROCESS

The manufacturing process took place in the Delft Aerospace Structures and Materials Laboratory (DASML) located at the Faculty of Aerospace Engineering, Technical University Delft. The preparation of the samples in the mold took place within a fume hood, and the actual pressing took place on the workfloor.

2.3.1. EQUIPMENT

Several pieces of equipment are required to successfully sinter the ceramics. First, a mold is required, in this case, a steel mold was manufactured specifically for this purpose. This mold had a chamber of 20 mm diameter where the samples were sintered. The other standard equipment needed for the preparation of the samples was a set of spatulas, a scale, tweezers, and a 1 mL syringe.

Beyond these standard materials, several other pieces of equipment were needed. In order to help remove the finished samples, small 22 mm diameter baking paper circles were punched out and used on the top and bottom of each sample. Small plastic lidded containers were used to mix the powder and solvent together. A photo of the setup needed to create the samples is shown in Figure 2.2.

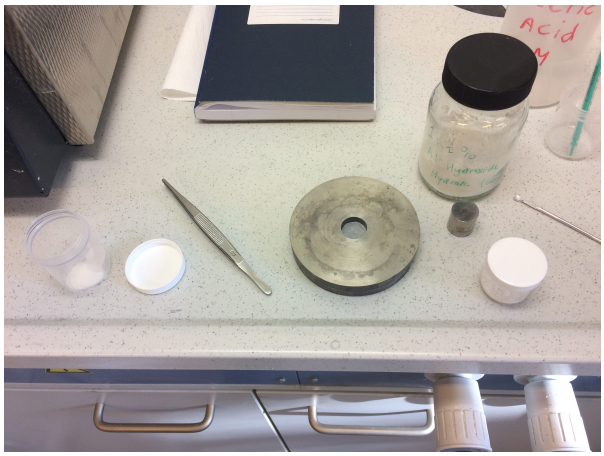

Figure 2.2: Required materials for the creation of ceramic samples. From left to right, baking paper circles, tweezers, mold, mixing container, powder, syringe in container, and acid container.

The sintering process took place in a 1000 kN Joos Press. In order to protect the plates of the press, aluminum blocks were used above and below the mold during the sintering process. This setup can be seen in Figure 2.3, where the mold is sitting on a thin aluminum plate, and an aluminum block is balancing on the top of the mold plunger.

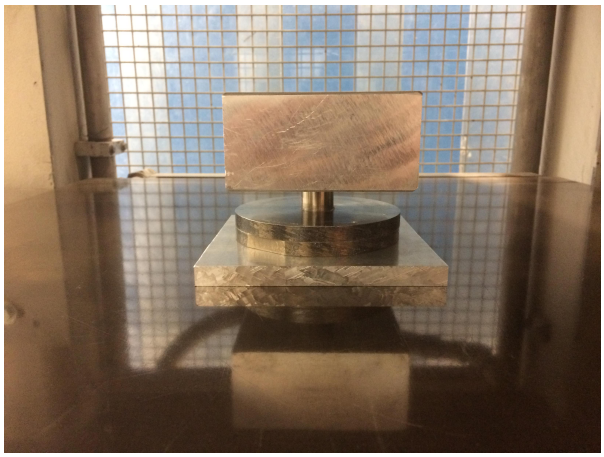

Figure 2.3: Setup of the mold on the lower Joos press plate before closure

As could be expected, adding that much material between the press plates and the mold does alter the heating profile of the mold. Based on some tests using a thermocouple, as shown in Figure 2.4, it was determined that it takes about 6 extra minutes to reach the final temperature, therefore, 6 minutes were added to the sintering time to allow the mold to get up to temperature. The actual sintering process was controlled by a set program within the Joos press, allowing for automated process control. The pressure, temperature and heating and cooling rates could all be controlled precisely.

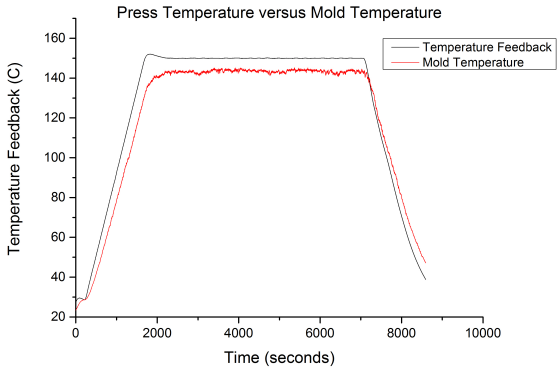

Figure 2.4: Feedback temperature of press versus the thermocouple measured temperature on the mold

There is a slight temperature variation (ca. 5 °C) at the max temperatures, which might be due to the fact that the thermocouple had to be placed on top of the mold where the plunger meets the upper plate and in contact with the atmosphere. This means that the temperature measurement is not taken exactly where the sample would be, and most likely the sample temperature will be higher.

After the sintering process, several more pieces of equipment are needed to remove the sample from the mold. It was found that after the sintering process the mold itself was very tightly stuck shut. It was impossible for the mold to be opened under just muscle power, so the addition of a plastic strap wrench shown in use in Figure 2.5 was needed. This tool made the opening of the mold go from almost impossible to quite simple.

Figure 2.5: Use of the Bahco plastic strap wrench in opening the mold after sintering

Once the mold was opened, the actual sample needed to be removed. This was done by using a hydraulic hand press, a washer, pipe and screw. The parts are shown in Figure 2.6, and the method for their use will be explained in the next section.

Figure 2.6: Bolt, washer and pipe used to take mold apart after sintering

When doping the zinc oxide powder, in order to mix the powders homogeneously, a Retsch PM100 planetary ball mill was used, as shown in Figure 2.7.

Figure 2.7: Planetary ball mill

The mixing parameters will be explained later in this chapter.

To conduct some of the other processes, a conventional furnace was used. The one used for the experiments was a Nabertherm P330 furnace, which can be seen in Figure 2.8.

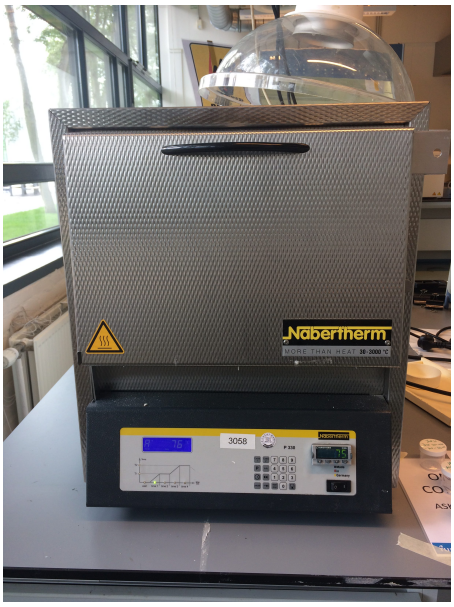

Figure 2.8: Furnace

This furnace has the ability to be able to be programmed, which assists in being able to have more specific heating profiles and to be able to run tests overnight.

2.3.2. PROCESS

Determining the most effective process for sintering took a number of attempts and trials. This section will illustrate the most effective method used to manufacture the samples. This process was the same for all samples, including the measurements of powder and liquids.

First, the mold must be prepared. This is done by taking the lower half of the mold and placing one of the 22 mm diameter baking paper circles on the center post, as can be seen in Figure 2.9.

Figure 2.9: Placement of the baking paper circle

Initially, the paper circles were only 20 mm, so exactly the same size as the sample, and 25 mm diameter circles were also tried. The 25 mm circles were too large, allowing for too much overlap outside of the sample, and were too large for the upper surface, causing problems with the sample quality. the 20 mm diameter circles were used for the majority of the samples, as they easily fit into the mold. One drawback was found, and that was due to their exact fit and the fine powder size, there would be leakage of the powder-solvent mixture between the two plates, and if the pressure was high enough, the entirety of the mixture would squeeze out. This was the same for the upper layer, that with the 20 mm diameter circles there was significantly more oozing of the paste out around the plunger. The 22 mm circles took the best of both, preventing the oozing of the paste in between the two mold halves, as well as not being too large for the placement of the plunger.

Once the circle was placed, the upper part of the mold could be placed on top, taking care that the baking paper circle was still centered. The two parts of the mold were fitted together, and pressed together by hand until they had a tight fit. During this pressing, the paper circle will be pressed between the two plates. Care should be taken to check that the paper is flush to the bottom post, like in Figure 2.10.

Figure 2.10: Paper circle after fitting of the upper mold

Once the two halves of the mold are together, the powder can be measured out and the solvent added. This mixing process is done in a small closed plastic jar, as seen in Figure

2.11, to prevent inhalation when moving from the fume-hood to the scale, as well as ease of mixing. All samples were created with a 20 weight percent ratio, therefore 2.5 grams of powder were mixed with 0.5 mL of acetic acid. The 1 mL syringe was used to measure out the acid and drip it on the powder to prevent powder from leaving the container.

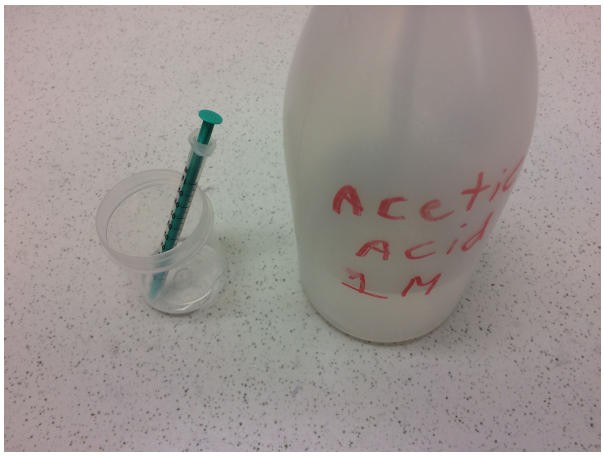

Figure 2.11: Tools needed to add the acid solution into the powder

The syringe allowed for precise measurements as well as an ease of adding the acid to the powder without there being powder escapage. However, if the acid is expelled too quickly from the syringe, the increased flow will cause some of the powder to spill out of the container. Once the acid is added, the mixture is mixed with a flat spatula until the mixture appears homogeneous. The mixture is then spooned into the mold and pressed down so that it is below the top of the mold, as seen in Figure 2.12. The upper baking paper circle can be seen on the edge of the mold.

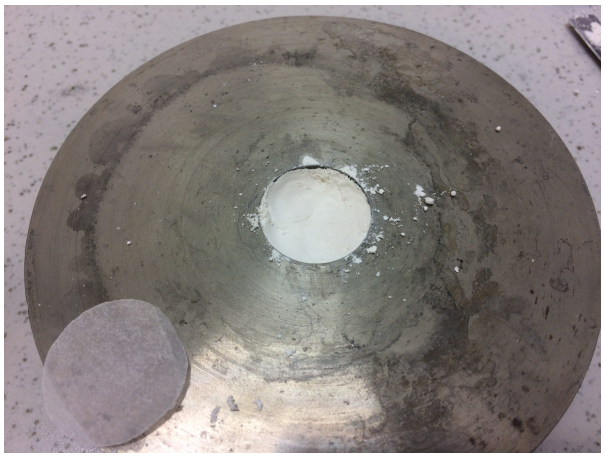

Figure 2.12: Mold filled with the powder/solvent mixture

Once the mold is filled, the second baking paper sheet needs to be added to the system. This can be placed with tweezers or by hand, taking care that once the paper touches the paste it will start to curl, the start of which can be seen in Figure 2.13, so these next steps should be completed relatively quickly.

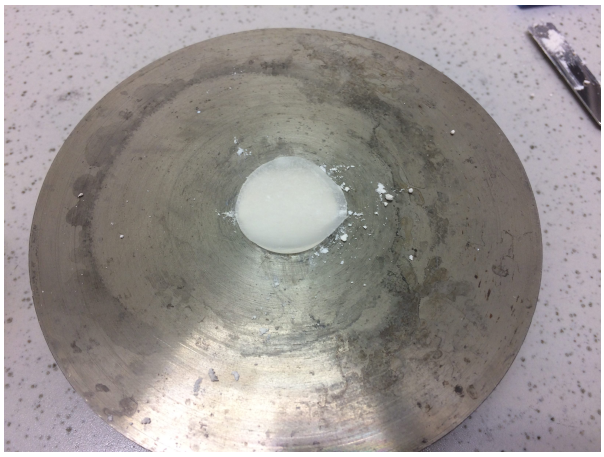

Figure 2.13: Mold prepared for plunger with second paper circle on the top of the paste

Once the paper circle is placed on the opening, the hardened steel plunger should be fit by hand as seen in Figure 2.14, taking care to insert it as straight as possible. If it is not inserted correctly, it can cause permanent damage to the mold.

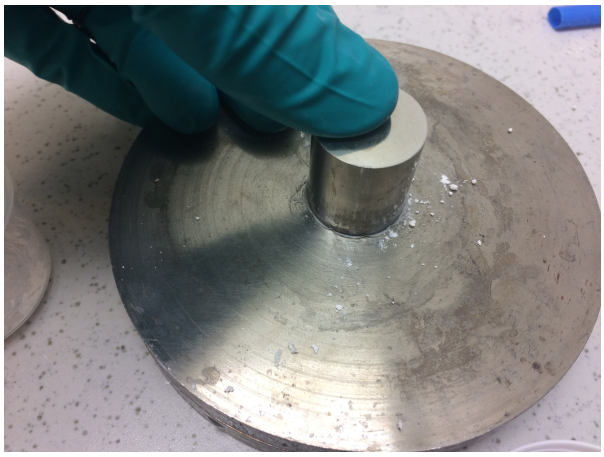

Figure 2.14: Hardened steel plunger being press fit into the mold by hand

In most cases, the plunger was not as straight as it should be, which would not be acceptable for it to be placed into the Joos Press as is. This next step acts with a double duty, to straighten the plunger, and to compact the powder a bit to limit the amount of paste which will ooze out in the later process. Once the plunger was press fit by hand, the entire mold was then placed into a hand hydraulic press and was tightened, being careful to keep the mold in the center of the upper screw, as can be seen in Figure 2.15. The plunger is already straightened at this point.

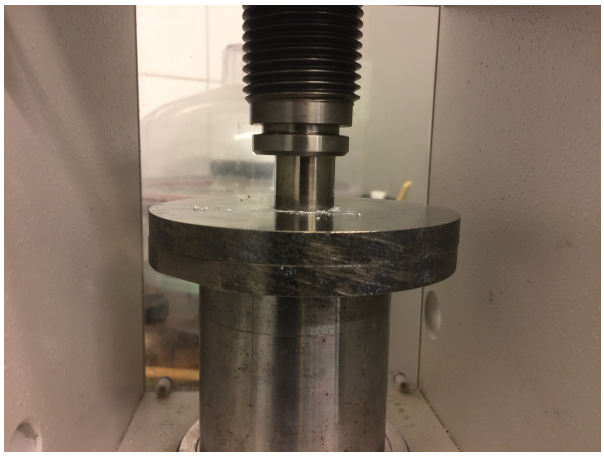

Figure 2.15: Mold in place within the hand hydraulic press

Once the mold is secure, the hand hydraulic press is used to compact the powder, stopping the moment there is a force reading on the dial. The point of this was to make a pellet before the sintering pressure, and it was found to improve the final product. The mold was then removed from the press, and cleaned with a damp paper towel to remove any remaining paste on the surface. Once this was completed, the mold and aluminum blocks were taken to the Joos Press and placed on the bottom plate. Figure 2.16 shows the first protective aluminum plate with the mold on top.

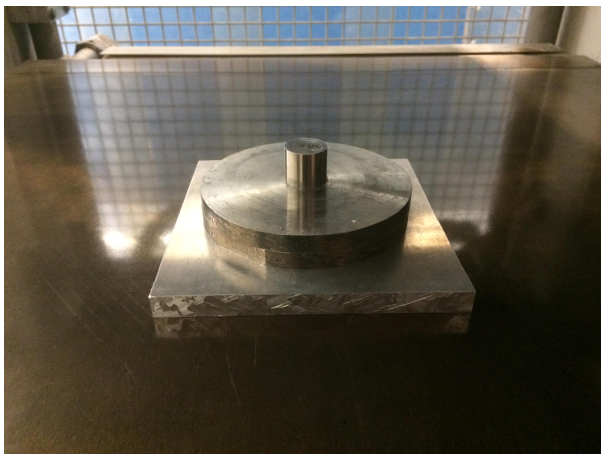

Figure 2.16: Mold in place in Joos Press with bottom protective plate

From this point, the top protective block was added on top of the mold plunger. This block needs to be balanced on top of the plunger, so to give an idea of the center of the block, it was marked with permanent marker, as can be seen in Figure 2.17.

Once the block is balanced on the top of the plunger, if it is properly centered, as was shown back in Figure 2.3, the press can be closed with no fear of the block falling off. Ideally, when the plates come together, the upper block should not shift, but it can be that is it not completely flat and therefore will align slightly. This alignment should not be in more than one direction or more than about a millimeter.

Once the press is closed, the proper program can be loaded and the sintering process started. The Joos press is quite simple in its use, it can apply a pressure and temperature

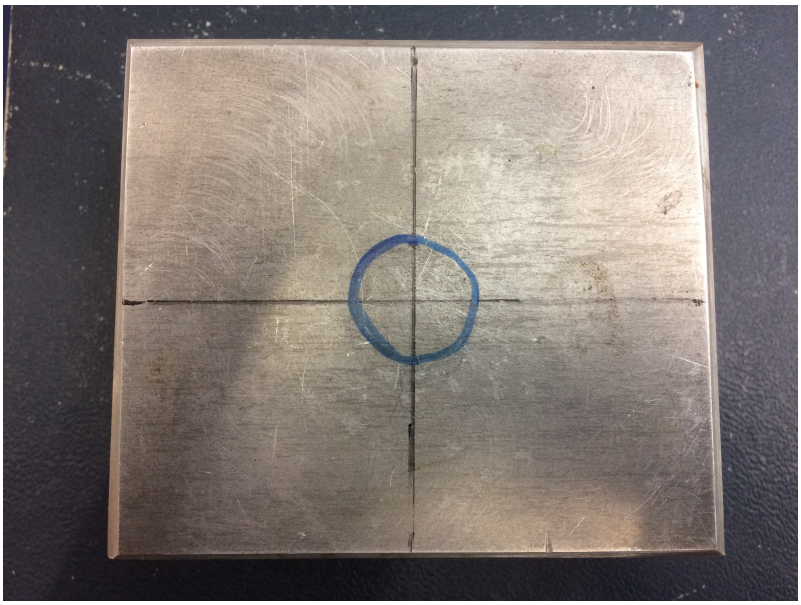

Figure 2.17: Markings on the upper aluminum block

according to manual input or a pre-set program. For the case of the cold sintering, a program was used with the needed temperature and pressures indicated within the program, as shown in Figure 2.18. When this press is normally used, the upper area of the press would be used as an input for the program, but since the diameter is so small at 20 mm, it triggered the safety protocols and the press would not apply pressure. To overcome this, the lower area of the mold was used instead, which had a diameter of 100 mm. As long as the protective blocks are always used when sintering in the Joos press, it should not cause any problem.

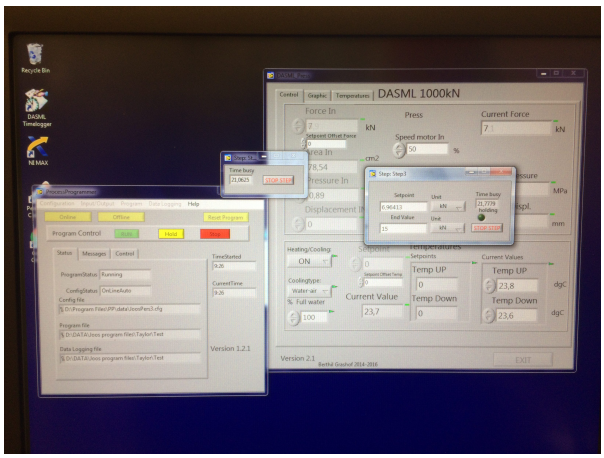

Figure 2.18: Sintering Program running on the Joos Press

Once the program is finished, the press can be opened again and the mold removed. It was found that the most effective way to then open the mold was to use the plastic strap wrench around the upper half of the mold while the bottom was clamped in a bench vice. This process was shown in Figure 2.5. Once the mold was loosened, it could be opened by hand and the ceramic pellet seen. A few more steps are required though to free the pellet

from the mold with the least amount of damage. The hand hydraulic press is then required, first with a washer that has an inner diameter larger than the pellet size and smaller than the upper press screw. After that, the plunger of the mold needs to be removed, this time by using a piece of pipe around the plunger and a bolt to allow for only supporting the plunger during the pressing. The setup with the press and washer is shown in Figure 2.19, and the press, pipe and bolt setup is shown in Figure 2.20.

Figure 2.19: Use of washer to remove sample

The washer was used to allow the press to press only on the upper plate (the plate directly under the washer in the photo. This method was found to cause the least amount of damage to the sample. It takes about 20-25 pumps of the press handle to get the sample high enough to be removed.

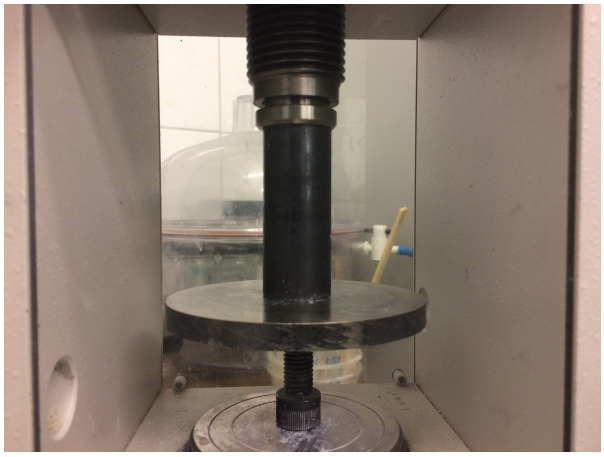

Figure 2.20: Use of pipe and bolt in the removal of the plunger

To then remove the plunger from the upper part of the mold, the same principle is then applied. This time the pipe presses on the upper plate only, while the bolt supports the plunger, allowing for the upper plate to be easily pressed off of the plunger. After use, the mold needs to be wiped down to remove any excess material on the material.

It was found that after a month that the samples were always breaking when being removed from the mold. It was thought that it was due to a sort of fatigues of the mold material. However, this problem was not resolved even when the mold was refurbished, so in the

end the solution was found to actually reverse the upper part of the mold. Once this part was flipped upside down, the manufacturing problems were resolved. Even though the mold was used intensively in this flipped position, the problem never reoccurred during the remaining manufacturing process.

2.3.3. MEASUREMENT EQUIPMENT

Three measurements were taken on the samples, density, x-ray diffraction measurements, and Broadband Dielectric Spectroscopy. Scanning Electron Microscope Images were also taken of many of the samples to analyze the microstructure.

For the vast majority of samples, particularly the pure zinc oxide samples, the density was taken using the measured volume and mass of the sample. This was due to the fact that the samples were so brittle, and in many cases the samples would flake apart soon after taking these measurements. Using a micrometer, the thickness was taken. This thickness was then used with the area of the sample to calculate the volume and then the measured mass was used to calculate the actual density of the sample. The theoretical density was then used to calculate the density of the samples.

For the samples which could withstand the measurement method, the Archemedes method was also used, the setup from Mettler-Toledo can be seen in Figure 2.21.

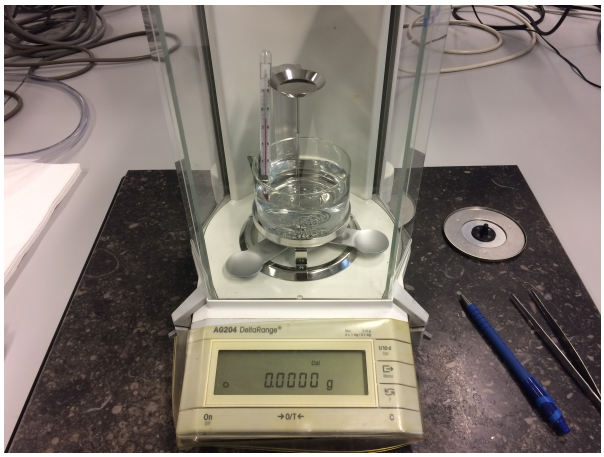

Figure 2.21: Archimedes setup for measuring density

From this measurement method, the dry and wet weights are obtained, as well as the temperature of the water. Using the temperature of the water, the precise water density can be calculated, and from there, the following equation can be used to determine the density of the sample.

$$\rho = A/(A-B) * (\rho_0 - \rho_L) + \rho_L \tag{2.1}$$

Where:
ρ = Density of the sample
A = Weight of the sample in air
B = Weight of the sample in water
ρ_0 = Density of water
ρ_L = Density of air($0.0012 g/cm^2$)

This method requires that the air bubbles are completely out of the sample for the immersion within the water. For some samples, this was more difficult, as the sample seemed to be relatively porous.

X-ray diffraction (XRD) was also used for measuring the final ceramic samples. The equipment used was a Rigaku Miniflex 600 using Cu Kα radiation, shown in Figure 2.22. The use of this was to confirm what the final ceramic was made up of, to determine if there had been any contamination or unexpected reactions within the material during the cold sintering process.

Figure 2.22: Rigaku Miniflex 600

Electrical measurements were taken using a Agilent high resistance meter (4339B) and component test fixture (16339A). Direct current resistance values were used to determine the effect of the dopant on the zinc oxide ceramic's electrical properties. A picture of the setup can be seen in Figure 2.23.

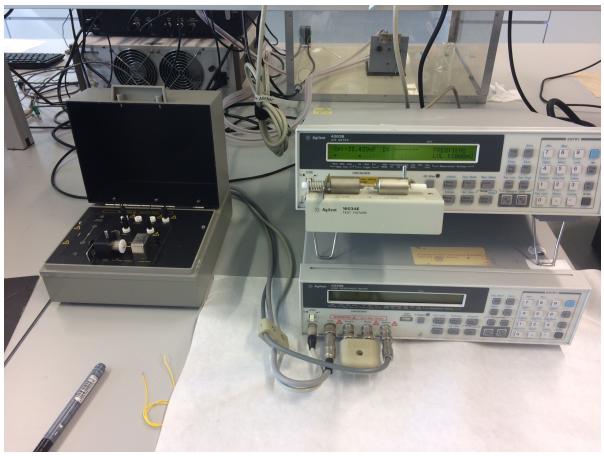

Figure 2.23: Agilent high resistance meter (lower right) and component test fixture (left)

Finally, scanning electron microscopy was conducted using a JEOL JSM-7500F microscope. The microscope also was equipped with energy-dispersive x-ray spectroscopy.

2.4. DOPANTS

Using added dopants allowed for the addition of aluminum within the ceramic system. As was explained earlier in this report, the addition of aluminum allows for the improvement of the zinc oxide's electrical characteristics, allowing for better functioning of the varistor properties. While there are several various dopants which could have been used to improve these properties, aluminum was chosen due to the fact that it is a relatively simple dopant, as well as having similar solubility in various pH systems as zinc.

Two forms of aluminum were used as dopants, Aluminum Hydroxide Hydrate and Aluminum Oxide. They were added in 1 weight%, 3 weight%, and 6 weight% to zinc oxide powder and ball milled in the planetary ball mill in a aluminum oxide container, with aluminum oxide balls. The solvent used was cyclohexane, and the milling parameters were 150 rpm for 1 hour. The mixture was then air dried in a fume hood until all of the cyclohexane evaporated.

2.4.1. ALUMINUM HYDROXIDE HYDRATE

The Aluminum Hydroxide Hydrate was ordered from Sigma-Aldrich (769460 Aldrich), and has a grain size of $< 45 \mu m$.

As can be ascertained by the name of this dopant, the actual chemical structure contains water, making the chemical formula $Al(OH)_3 \bullet H_2O$. The addition of the water will decrease the amount of Aluminum in a given mass of powder, so thermogravametric analysis was conducted to determine what percentage of the material was water. The graph can be seen in Figure 2.24.

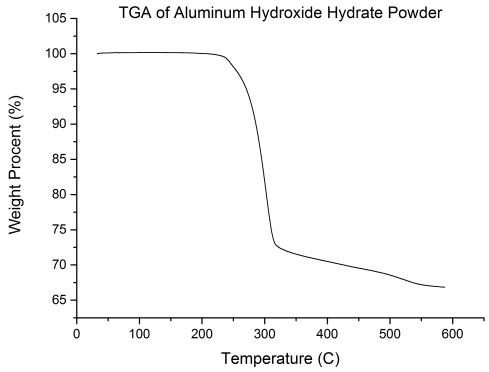

Figure 2.24: TGA analysis of the Aluminum Hydroxide Hydrate powder

The large dip in the weight at about 300 °C is the structural water evaporating from the system. This indicates that the amount of water is the system is about 30%. However, the amount of powder used to dope the systems was not changed, but this should be considered when looking at sample results when doped with Aluminum Hydroxide Hydrate.

2.4.2. ALUMINUM OXIDE

The aluminum oxide powder was ordered from Sigma-Aldrich as well (544833). This powder is a nanopowder, with a particle size of $< 50 nm$.

2.5. CONVENTIONAL SINTERING

As well as using cold sintering to manufacture the zinc oxide ceramics, a set of samples were also created using conventional sintering. To be able to have samples which can withstand the forming and initial firing process, 50g of the zinc oxide powder was mixed with 1.5g of polyethylene glycol which was dissolved in 10mL of warm water. This mixture was mixed in a large container, as can be seen in Figure 2.25.

Figure 2.25: Mixing of zinc oxide powder with solution polyethylene glycol

The mixture was mixed with the spoon until the powder was homogeneous and was formable. This homogeneous mixture was then pressed through a sieve to form granulates. From here, the powder was pressed in the same mold as what was used for the cold sintering samples. The same 2.5g of powder was used for each sample, pressed, and then collected for firing, as can be seen in Figure 2.26.

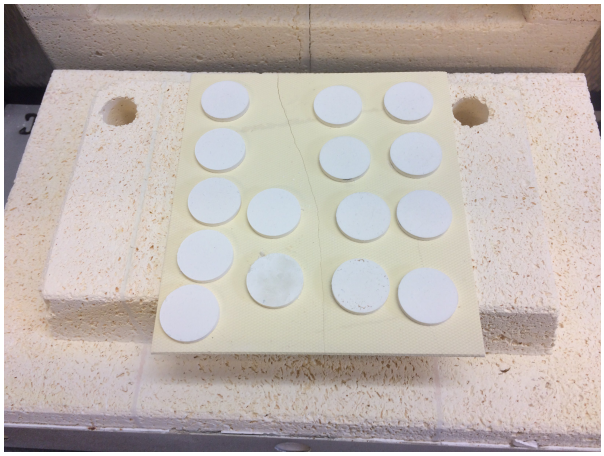

Figure 2.26: Pressed pellets ready to be fired

After all of the powder had been pressed, the samples were placed on a ceramic plate, as can be seen in Figure 2.26 and fired overnight. The firing process was conducted in steps, with a 6 hour ramp to 400 °C, a one hour hold, 3 hour ramp to 1100 °C, a 6 hour hold, and then cooling down. This can be seen in Figure 2.27.

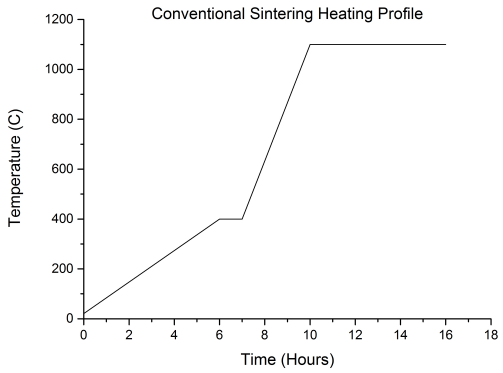

Figure 2.27: Conventional sintering method

Since there was the addition of the polyethlene glycol binder, during the firing process an extra step must be taken to first burn out the binder. This is the reason for the hour long step at 400 °C. The actual sintering process takes place at 1100 °C for 6 hours, chosen due to the literature of Mazaheri as well as Kundu Roy et al [37, 38]. This temperature and time was chosen as it should give a large final grain size as well as dense samples.

While all of the cold sintered samples were either white or grey in color, the conventional sintered samples were colored yellow, as shown in Figure 2.28, and were very dense with a density of 98.7%.

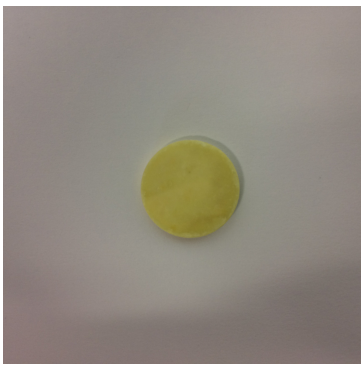

Figure 2.28: Conventional sintered zinc oxide ceramics

These conventionally sintered samples were used mainly to look at the microstructure, as well to see if it would be possible to cold sinter already sintered ceramics. For this process, a sandwich of two ceramic pellets were needed, which meant that the samples needed to be smooth one one side to try and limit the damage which would occur due to the added pressure. In order to get multiple samples which were all the same on one side, samples were taped using double sided tape onto a steel plate and then used with a polishing machine. The taped samples can be seen in Figure 2.26.

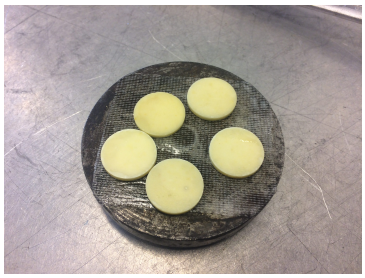

Figure 2.29: Conventional sintered zinc oxide ceramics taped to a steel plate

After the samples were polished, they were put in a small beaker of acetone and the beaker into the ultrasonic cleaner. This allowed for the simplest removal of the tape residue.

3

Zinc Oxide Based Ceramics

As literature concerning cold sintering is still quite sparse, the first step of this thesis was to determine the required process and parameters to create ceramics via cold sintering, using the paper from Funahashi et al. [32]. From here, the most promising parameters were selected for the manufacturing of the doped samples. Once a set of samples were created, various tests were conducted to be able to better compare the samples.

The zinc oxide ceramics were quite flakey and almost every single one fell apart or cracked at one point in the process. Possible reasons for this will be explained later in the report.

3.1. Optimization Process

The initial optimization process was based primarily on the density of the samples. As most reports in literature about ceramics was based on the density of the samples, this was found to be a good starting measurement which could be taken easily. The goal of the optimization process was to change the pressure and temperature to see what effect they had on the final density of the zinc oxide ceramic. For this initial optimization process, only the zinc oxide powder was used to create the samples.

Both the amount of solvent as well as the time were shortly explored during this process. For the solvent, going above 20 weight% turned the workable paste into a more glue like substance which would ooze out of the mold, leaving no remaining material in the sample area. The time was also increased in a couple of samples to determine if it would assist in the densification of the samples, but it was found to not have any improvement. The time of one hour was also preferred due to the ability to have fast manufacturing during the limited time of this project.

The first thing which needed to be checked was that there was no contamination or unexpected issue with the actual material of the final ceramic. This was done by using x-ray diffraction of the ceramic pellets. The results can be seen in Figure 3.1.

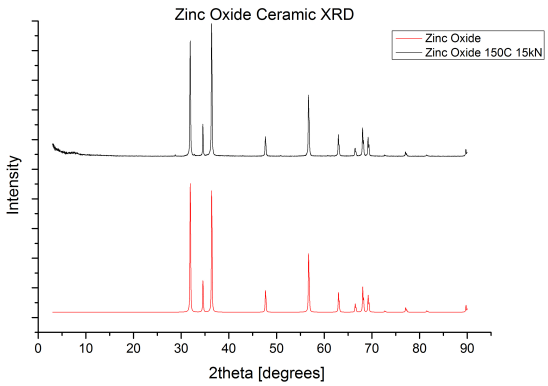

Figure 3.1: XRD of zinc oxide ceramics compared to theoretical

As can be seen, the measured diffraction pattern of the pellets matched the theoretical zinc oxide graph perfectly. There are also no extraneous peaks, meaning that there is no obvious contaminant, and the process can be confirmed to not adversely affect the material.

With the material confirmed, the density was then used to determine if there was an optimum for the temperature and pressure. The density was measured by volume and weight measurements instead of the Archimedes method due to the fragility of a large number of the samples, and the fact that some did not even survive the measuring with the micrometer.

The density was analyzed in relation to the temperature and the pressure.

3.1.1. EFFECT OF TEMPERATURE

For the temperature, a range of 126-190 °C was used, being above the vapour point of the solvent, and below the limit temperature of 200 °C. Figure 3.2 shows the measured densities of the samples in relation to the temperature of the cold sintering process.

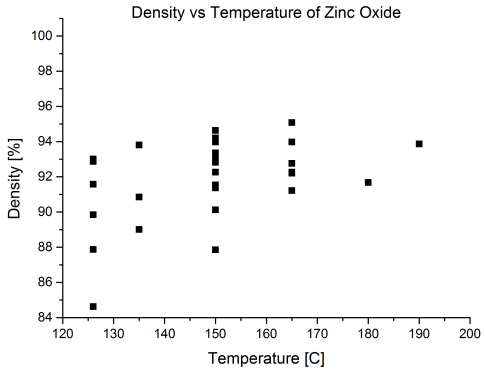

Figure 3.2: Temperature vs density of zinc oxide ceramics

It was found that within this range, the density was above 80%, however, there could be quite a variety within a certain temperature. Some of this was no doubt due to the applied pressures changing and perhaps some issues with the initial mixing or mold leakage, but

the values around 150-170 °C had better results. Temperatures above this point had no marked improvement in the density, and cost more time.

The quality of the samples did also improve as the project progressed, which could explain the cluster of samples with high density for the 150 °C sample set. These densities were also compared with some which could be measured by Archimedes method to see how the values compared. Figure 3.3 shows this graph, with the red values being the densities measured by Archimedes.

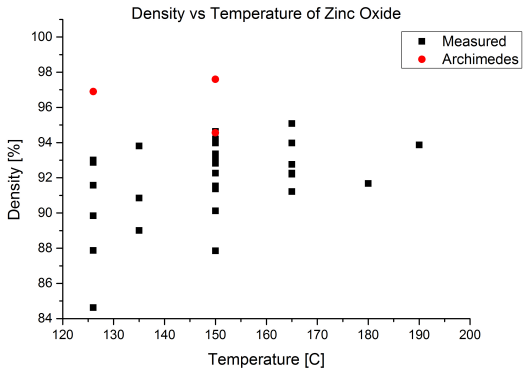

Figure 3.3: Temperature vs density of zinc oxide ceramics with Archemedes measurements

The values taken this way were normally higher than those taken by the measuring method, though at least the trend between 126 and 150 °C is similar. A more detailed comparison can be seen in Table 3.1.

Temperature [C]	Pressure [kN]	Density [%]	Archimedes Density [%]
126	15	92,9	96,9
150	15	92,8	97,6
150	15	87,8	94,6

Table 3.1: Comparison between measured and Archimedes densities

From this, the mid values of 150-165 °C were focused on for the future work. The samples made with 165 °C might have had slightly higher densities, however, the samples themselves were extremely flaky and not able to be used for any other tests. This can be seen in Figure

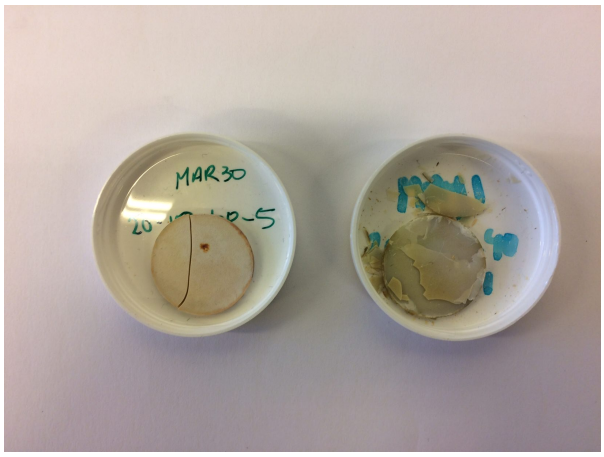

Figure 3.4: Comparison of 150 °C samples to the flaky 165 °C samples

3.1.2. EFFECT OF PRESSURE

The pressure was analyzed in a similar fashion. First, a large range of samples were created with varying pressures. The range used was 10kN - 25kN, as anything higher would cause the ceramic paste to ooze out of the mold completely, and anything less would not allow for sintering. Figure 3.5 shows the initial graph of the various pressures used and the resulting denisities.

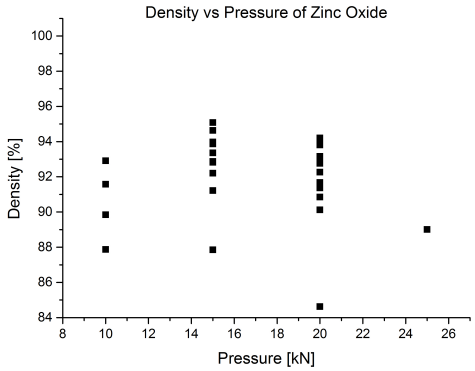

Figure 3.5: Pressure vs density of zinc oxide ceramics

The two forerunners were 15 kN and 20 kN with densities normally above 90 %, and while there is a slight difference in the densities, both of these pressures were looked at in more detail, which will be explained in the next section.

To look at the pressures in more detail, Figure 3.6 shows just the densities with the samples manufactured at 150 °C. Only 15 and 20 kN were used at this temperature.

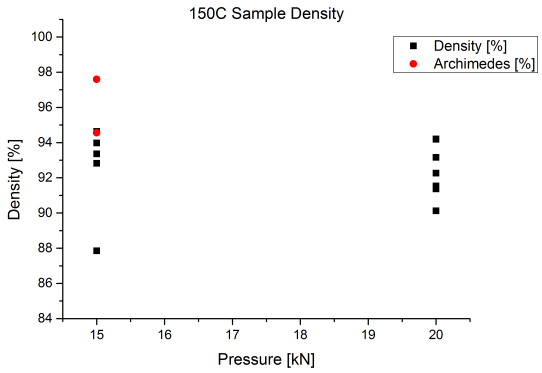

Figure 3.6: Densities of samples at different pressures manufactured at 150 °C

While there is one value at below 88%, the rest of the samples came out to be above 90% dense. In comparison, looking at the 165 °C samples in Figure 3.7, bearing in mind that the samples themselves flaked apart when picked up or any sort of force was applied to them, the densities are slightly different.

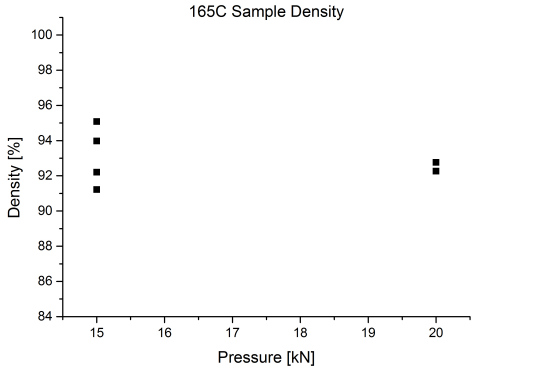

Figure 3.7: Densities of samples at different pressures manufactured at 165 °C

The samples manufactured at 165 °C were all above 90%, with one manufactured at 15kN being more dense than those sintered at 150 °C. However, the samples created at 20 kN were not so promising, and taking into account the flakiness of the ceramic when sintered at 165 °C, 150 degrees and 15 kN for the manufacturing was looking to be the forerunner.

3.1.3. FINAL OUTCOME AND PARAMETERS SELECTION

The final choice could not be done by density alone. As ceramics need to have a densifying action during the sintering process, this needed to be checked on the samples to determine if there was a clear forerunner. The scanning electron microscope was used to analyze the microstructure of the various samples to determine if there was a difference between the various process parameters. In an ideal situation, there would be grain growth, low porosity, and rounder but faceted grain shape. A number of different ceramics were placed under the microscope.

For the samples created at 150 °C, samples created at 10, 15, 20 and 25 kN were analyzed. Working from high to low, Figure 3.8 shows an overview of the sample fracture surface, and Figure 3.9.

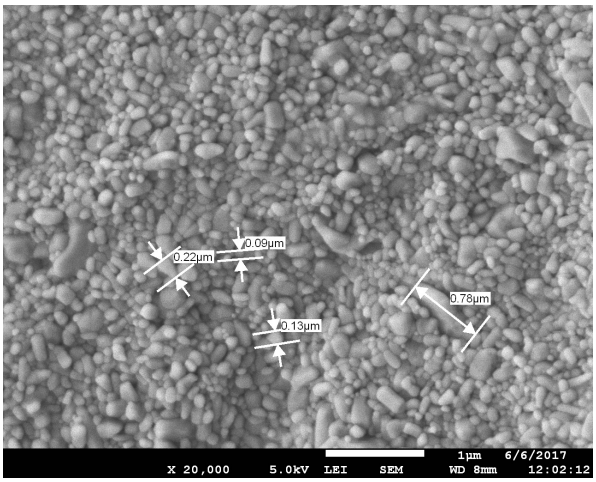

Figure 3.8: Zinc Oxide 150 °C, 25 kN, 20,000x

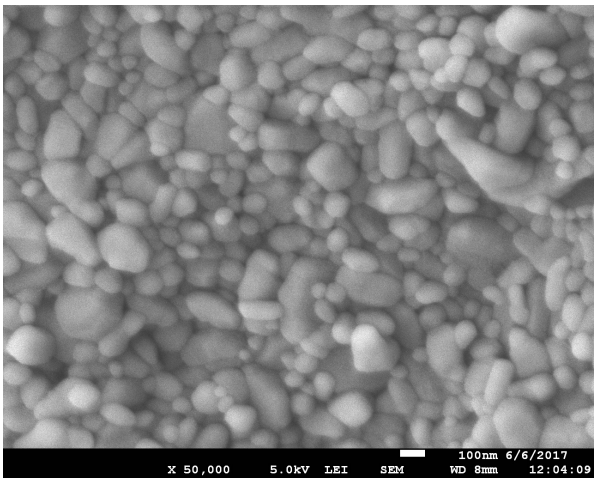

Figure 3.9: Zinc Oxide 150 °C, 25 kN, 50,000x

While there are some larger grains, the vast majority of them are still quite small, less than 0.25 μm. With a starting size grain of 0.04-0.1 μm, this was less than ideal. The grains themselves are still quite round, and not the more multifaceted grains which were expected.

Figure 3.10 shows an overview of the fracture surface of the 20 kN samples, and Figure 3.11 shows a close up of the grains.

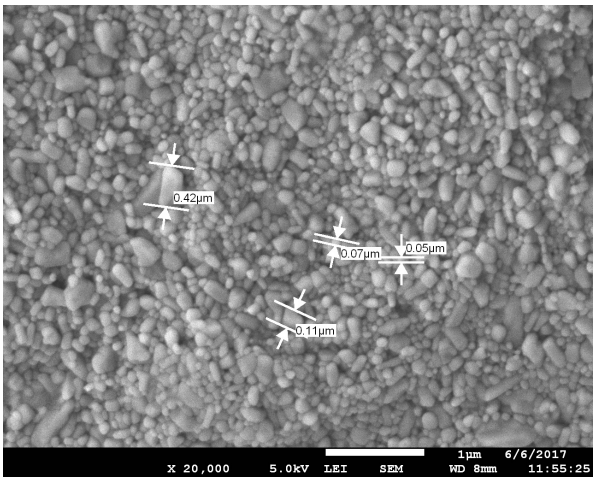

Figure 3.10: Zinc Oxide 150 °C, 20 kN, 20,000x

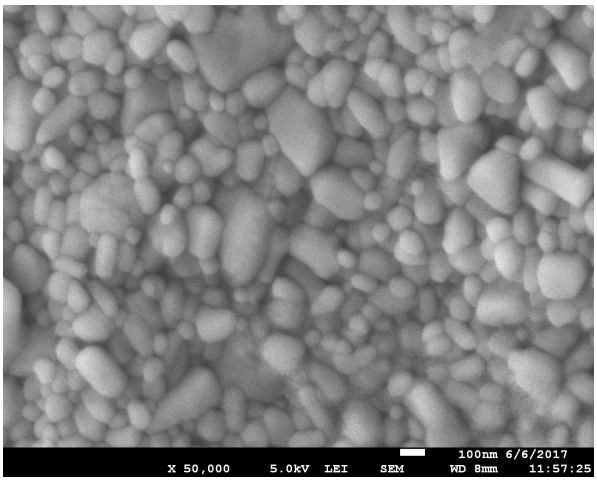

Figure 3.11: Zinc Oxide 150 °C, 20 kN, 50,000x

Overall, this microstructure looks very similar to that of the 25 kN sample, with small grains around 0.05-0.42 μm and no real faceted larger grains. This could perhaps explain some of the flakiness experienced by the samples. Moving to the 15 kN samples, Figure 3.12 shows the overview and Figure 3.13 shows the grains up close.

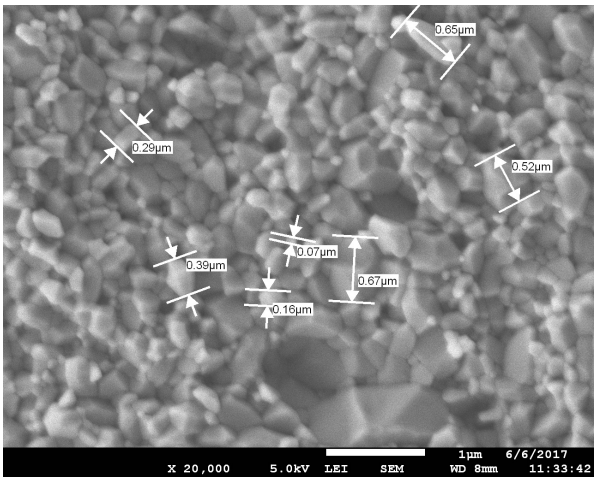

Figure 3.12: Zinc Oxide 150 °C, 15 kN, 20,000x

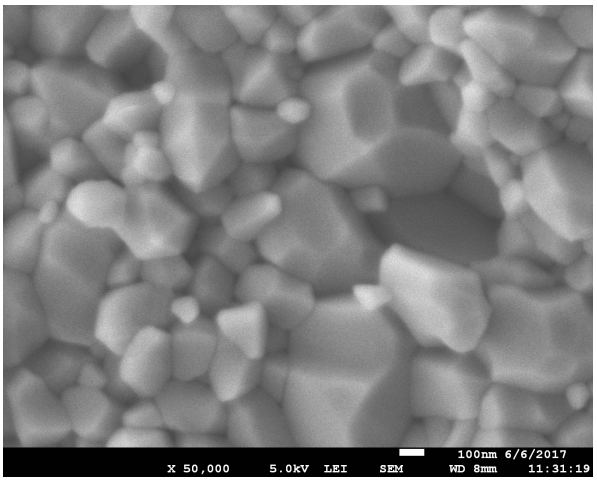

Figure 3.13: Zinc Oxide 150 °C, 15 kN, 50,000x

This type of grain growth and shape is much closer to what was expected from a sintering process. The grains are larger, and have a faceted look, showing that some of the grains have actually come together to form larger grains. There are still some smaller grains around 0.05 μm, but now there are many more in the range of 0.52-0.65 μm. So the question was if the lower pressure actually assist in forming the grains. From this idea, the 10 kN sample was also analyzed. Figure 3.14 shows the overview and Figure 3.15 shows the close up of the grains.

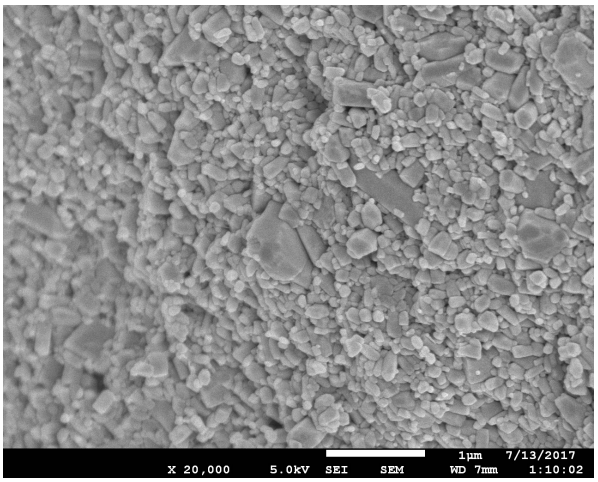

Figure 3.14: Zinc Oxide 150 °C, 10 kN, 20,000x

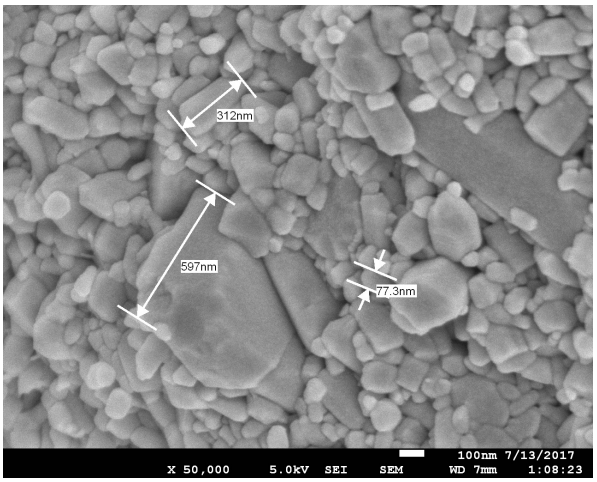

Figure 3.15: Zinc Oxide 150 °C, 10 kN, 50,000x

Unfortunately this does not seem to be the case. The grain size for the 10 kN samples are small, and while there is some of the faceting of the grains, it is not as developed as the 15 kN sample.

So, from the analysis of the microstructure, the decision to use 15 kN with 150 °C in the manufacturing can be confirmed.

3.2. ADDITION OF DOPANTS AND CHARACTERIZATION

Once the parameters were chosen using the zinc oxide ceramics, the doped samples were created. Using the ball milled powders, samples using the same 20 wt% acetic acid were

created.

The parameters which were used to sinter the samples were the previously mentioned 150 °C and 15 kN pressing for one hour. This set of parameters were used due to the fact that the doped samples were still mostly zinc oxide, and that the solubility of the aluminum allowed for dissolution within an acidic solution. However, it could be that these parameters are the most optimum for every zinc oxide based ceramic, but for the purpose of this thesis, they will suffice.

Once the doped samples were manufactured, measurements were taken, to compare their properties to those of the pure zinc oxide as well as to each other.

3.2.1. DENSITY

The density of the samples were measured mainly by measurement, however a set were measured by the Archimedes method to compare. While these samples were less brittle, the 1 wt% and some of the 3 wt% doped samples still had somewhat of a brittleness problem.

Starting with the aluminum hydroxide hydrate doped samples, Figure 3.16 shows the measured densities as well as those measured with Archimedes.

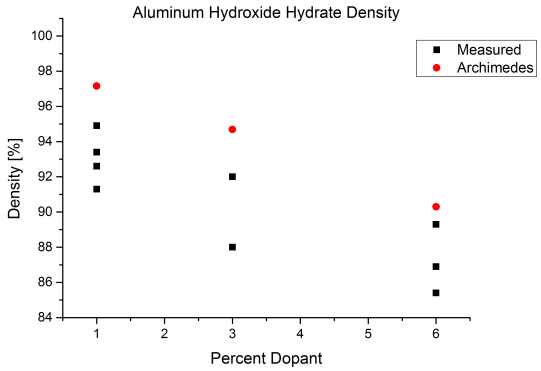

Figure 3.16: Density of aluminum hydroxide hydrate doped ceramics

During the water immersion, the samples emitted some bubbles, but after about 20 seconds it stabilized enough to take a reading on the scale. The trend seen in the aluminum hydroxide hydrate doped samples is that the density decreases down from the low 90% to the high 80% as the percent of dopant increases. This could mean that when the density is lower, the samples themselves are less brittle.

This trend is also seen for the aluminum oxide doped samples, seen in Figure 3.17. These samples also emitted bubbles when immersed in the water, but the Archimedes results are closer, especially for the 3 wt% samples.

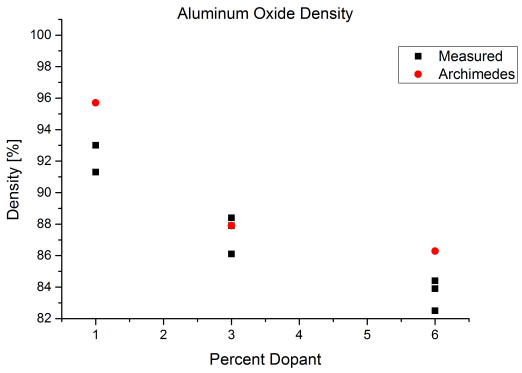

Figure 3.17: Density of aluminum oxide doped ceramics

In both cases, the density of the 6wt% samples were the lowest, however, they were still in the high 80%. It might also be the case that the addition of more dopant means that the processing parameters need to change a bit in response which could cause lower densities.

3.2.2. X-RAY DIFFRACTION

For these samples as well, the first test which was conducted was x-ray diffraction of the various weight percents and dopants. This was to confirm that the ceramics consisted of the expected materials, and to see if any phase information could be gained.

The expectation for this was that there would still be some visible dopant in the XRD measurements, causing a mix of the two diffraction patterns. Starting with the aluminum hydroxide hydrate, Figure 3.18 shows the overall diffraction patterns in comparison to the measured zinc oxide sample.

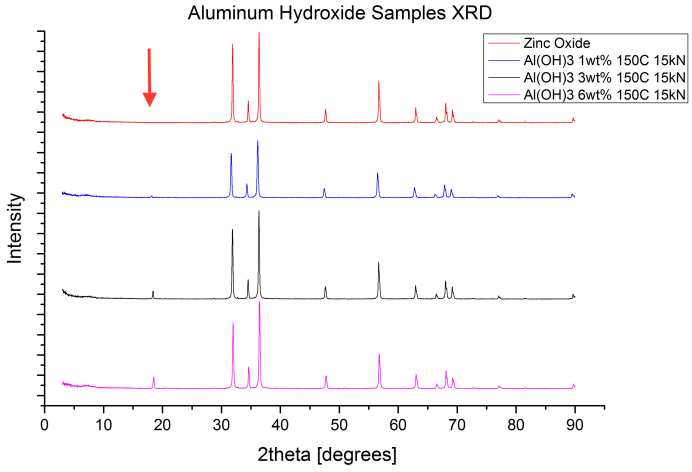

Figure 3.18: X-ray diffraction of aluminum hydroxide hydrate doped samples

While the vast majority of the diffraction patterns matches the zinc oxide ceramic, there is still a peak on the left of the graph which grows as the weight percent of the dopant increases. As there is this increase, it is expected to be related to the dopant itself, which, as

shown in Figure 3.19, ends up to be Gibbsite, or aluminum hydroxide.

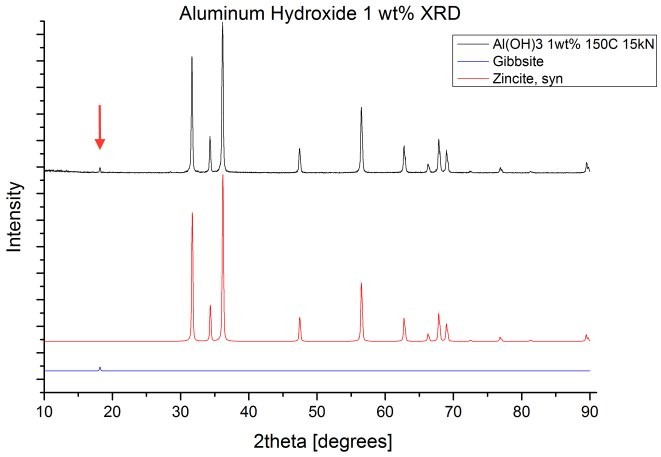

Figure 3.19: X-ray diffraction of aluminum hydroxide hydrate doped sample compared to theoretical

The Gibbsite pattern matches the small peak on the left (with arrow), meaning that there is still some aluminum hydroxide left after the sintering process. More importantly however, this also indicates that there is no indication of a third phase within the material.

The aluminum oxide doped samples were analyzed in a similar fashion. Figure 3.20 shows the doped diffraction patterns in comparison to the zinc oxide material.

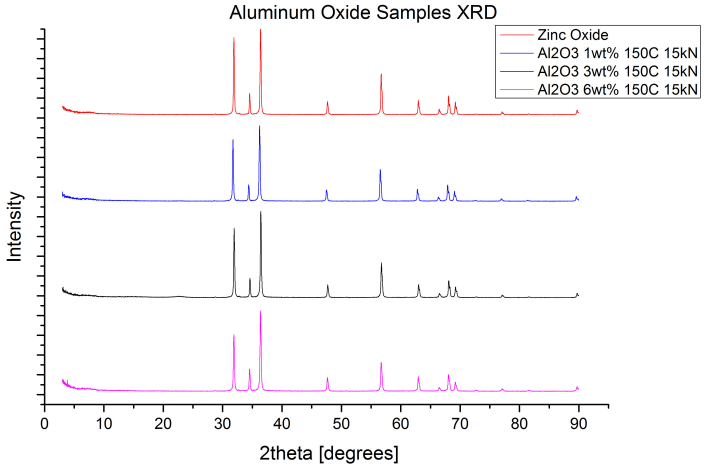

Figure 3.20: X-ray diffraction of aluminum oxide doped samples

For this material, there is no visible difference between the various patterns, which is due to a very simple reason. It was found that aluminum oxide has peaks in the same 2θ as zinc oxide. This can be seen in Figure 3.21 where the measured and theoretical diffraction patterns are graphed.

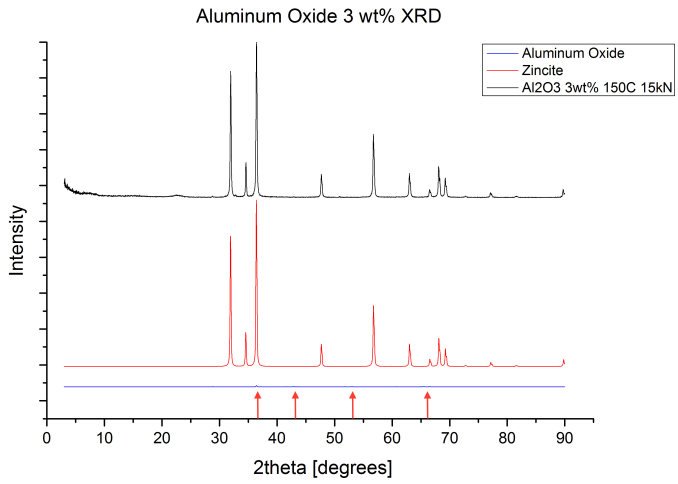

Figure 3.21: X-ray diffraction of aluminum oxide compared to theoretical

First off, the peaks for the aluminum oxide have a very low intensity (marked with arrows), and secondly, they match up with the very large peaks of the zinc oxide, meaning that they will be swallowed up by these larger peaks on the combined XRD diffraction pattern.

In conclusion, the XRD diffraction patterns were as expected, meaning that there should be no third phase present in the final ceramic, and that there is no visible contamination. From this, it was decided that the samples were of sufficient quality to continue with the characterization.

3.2.3. SCANNING ELECTRON MICROSCOPY

Since the materials were found to be as expected with no extraneous phases, the microstructures were analyzed using the scanning electron microscope. Two types of samples were analyzed, the raw fracture plane of the material, and a set of samples were embedded into resin and polished to look at the clean surface of the material.

FRACTURE PLANES

For each of the ceramic types, a small piece was fractured off of the bulk, and analyzed under the scanning electron microscope. Starting with the 1 wt% samples, Figure 3.22 shows the grains on the fracture plane for the aluminum hydroxide hydrate samples, and in comparison, Figure 3.23 shows the same for the aluminum oxide sample. In comparison, all of the doped samples have smaller grain sizes than that of the equivalent zinc oxide ceramics, which further indicates that perhaps the sintering parameters do need to change whenever the material composition changes.

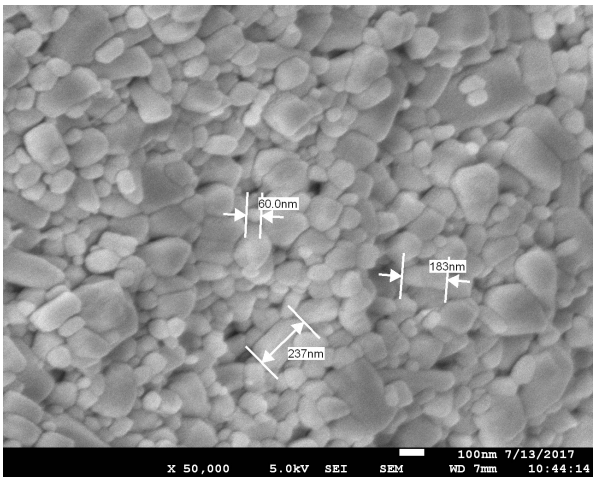

Figure 3.22: Aluminum hydroxide 1 wt% 50,000x

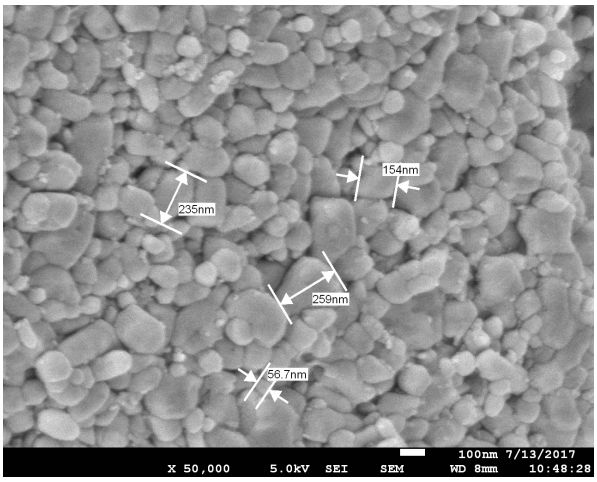

Figure 3.23: Aluminum oxide 1 wt% 50,000x

The grains with the 1 wt% are almost all below 300 nm in size, slightly larger than the original grain size of the powder, but not as large as would be expected from a sintered ceramic. The grains are still quite round, and are not as faceted as they could be, although they are larger than those of the zinc oxide ceramics sintered at the other parameters. Moving to the next dopant amount, Figure 3.24 shows the microstructure of the 3 wt% aluminum hydroxide sample, and Figure 3.25 of that of the aluminum oxide doped material.

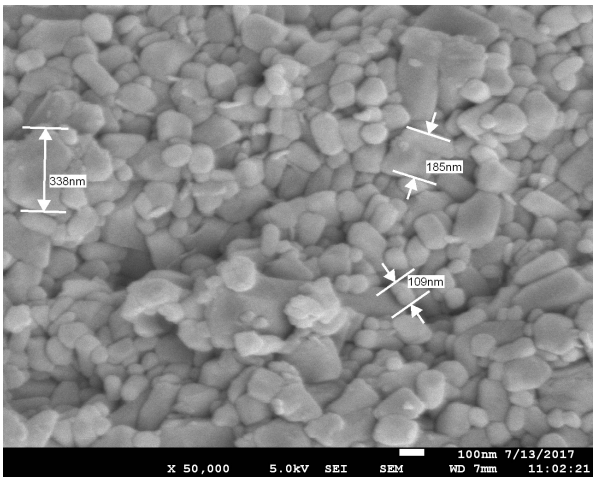

Figure 3.24: Aluminum hydroxide 3 wt% 50,000x

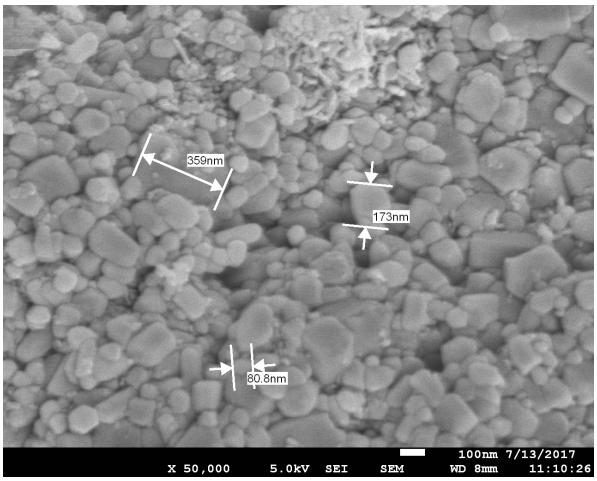

Figure 3.25: Aluminum oxide 3 wt% 50,000x

These 3 wt% doped systems look similar to those of the 1 wt% system, which most likely is due to the fact that it was only a 2% increase of dopant. The addition of more dopant does not seem to have any more of an effect on the grain size compared to the zinc oxide ceramic, at least in this step from 1 to 3 wt%, The grains are still relatively round. Finally, the samples with 6 wt% dopant were analyzed. Figure 3.26 shows that of the material doped with aluminum hydroxide hydrate, and Figure 3.27 shows the aluminum oxide version.

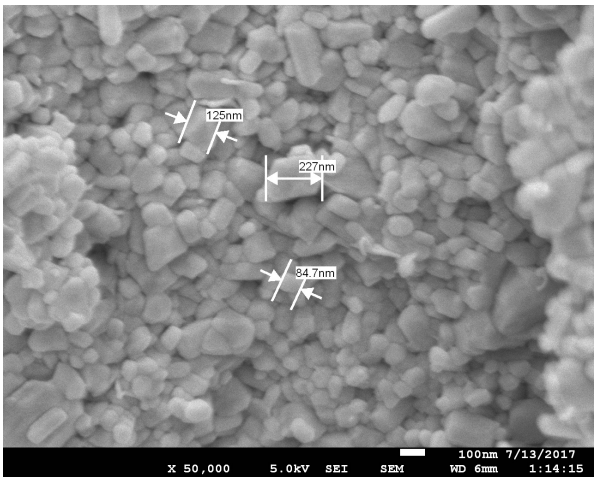

Figure 3.26: Aluminum hydroxide 6 wt% 50,000x

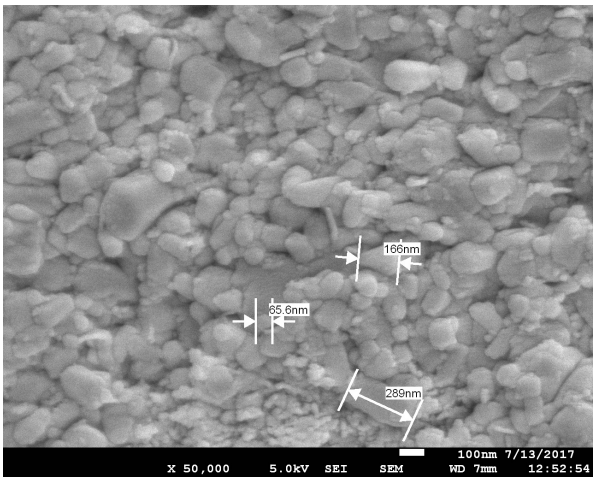

Figure 3.27: Aluminum oxide 6 wt% 50,000x

The aluminum hydroxide hydrate ceramic looks relatively the same as the previous wt% samples, however the aluminum oxide sample is showing more small particles between the larger grains. As the original powder had a grain size of $< 50nm$, it could be that these small grains are the zinc oxide material. It appears as though the act of doping the material has more effect on the grains than the exact dopant used, given that the solubility rules are followed.

EMBEDDED AND POLISHED SAMPLES

For the polished samples which were embedded in resin, the goal was to see if it could be determined where the dopants were after the sintering process. To compare them as well to the zinc oxide ceramic, Figure 3.28 shows the overview of the polished samples.

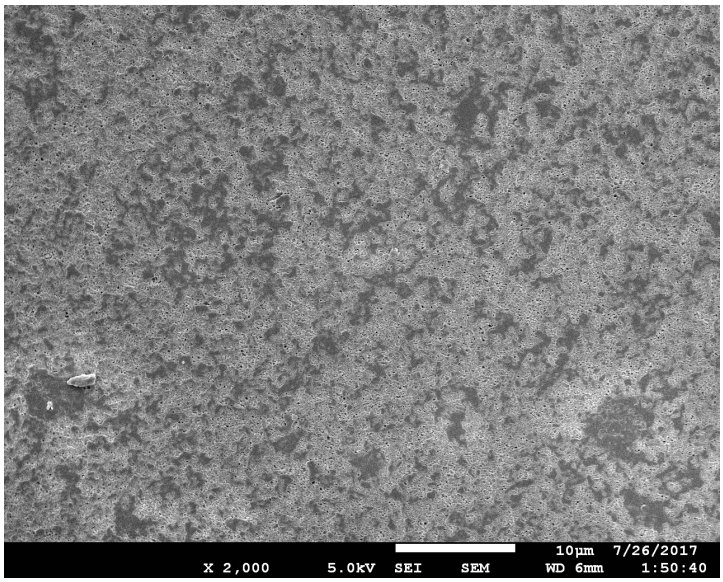

Figure 3.28: Polished cold sintered zinc oxide ceramic face 2,000x

The sample itself is quite homogeneous, with the polishing showing the insides of some areas, with some smaller darker areas scattered around the surface of the material. In comparison, Figure 3.29 and 3.30 show the faces of the two doped materials.

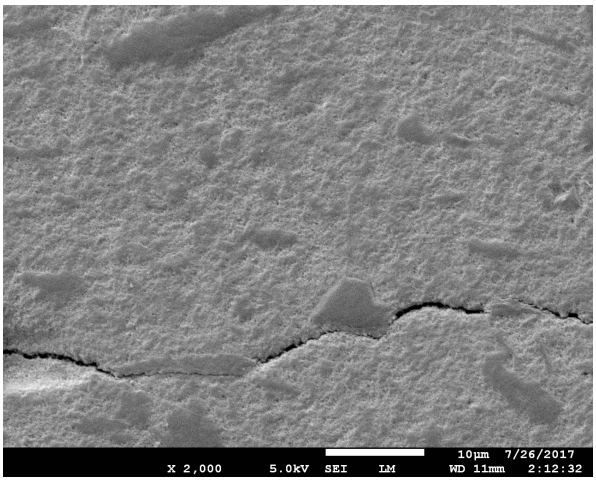

Figure 3.29: Aluminum hydroxide 6 wt% 2,000x

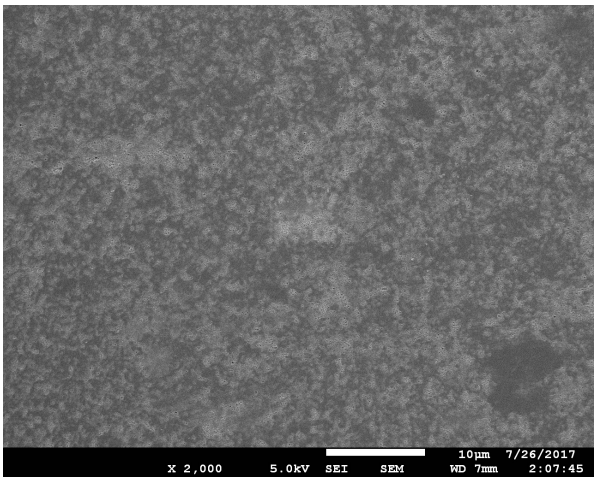

Figure 3.30: Aluminum oxide 6 wt% 2,000x

In both of these, though more easily seen in the aluminum hydroxide hydrate doped sample, there are larger dark areas, with the rest of the material looking relatively homogeneous. In order to have a better idea of what these dark areas are, energy-dispersive x-ray spectroscopy (EDS) was done on these materials. Figures 3.31 and 3.32 are the original SEM images which were taken at 50,000x.

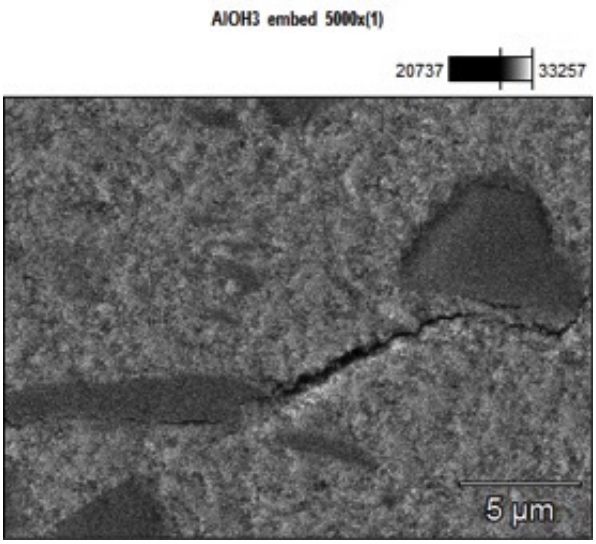

Figure 3.31: Scanning electron microscope image of 6 wt% aluminum hydroxide 5,000x

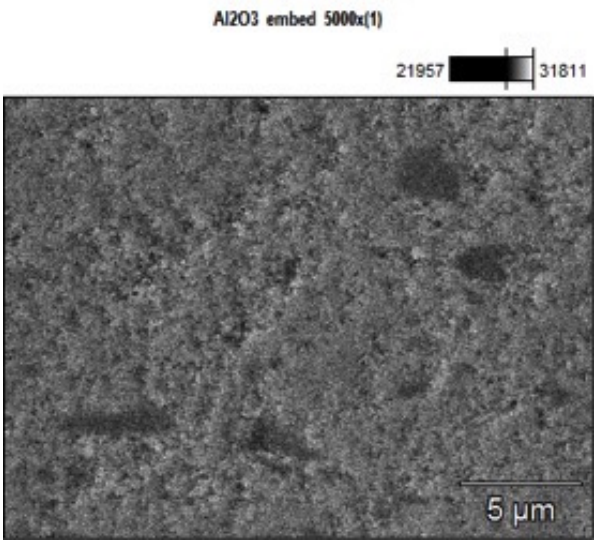

Figure 3.32: Scanning electron microscope image of 6 wt% aluminum oxide 5,000x

In both of these images, there are dark areas visible in the photo, and particularly in the case of the aluminum hydroxide hydrate sample, there is a crack running through the lighter areas, which goes around these dark patches. It was expected then that these dark areas would have a different composition to the bulk material property. Figures 3.33 and 3.34 show the results for the zinc distribution, and Figures 3.35 and 3.36 show the same but for aluminum.

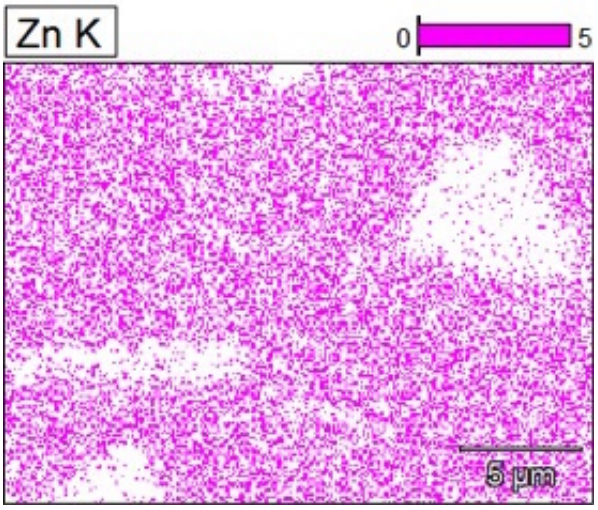

Figure 3.33: EDS results for zinc on Figure 3.31

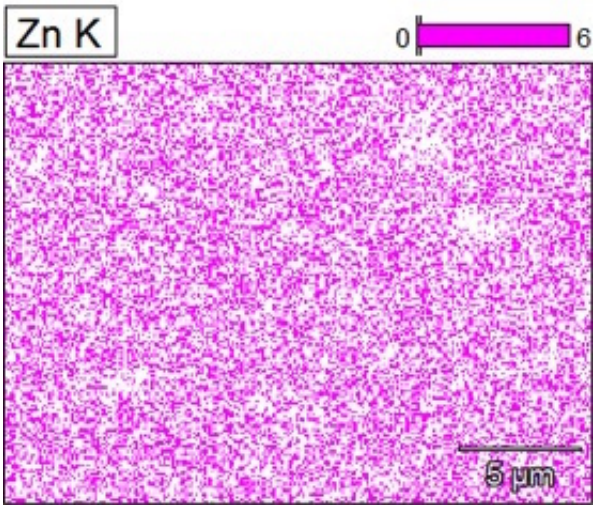

Figure 3.34: EDS results for zinc on Figure 3.32

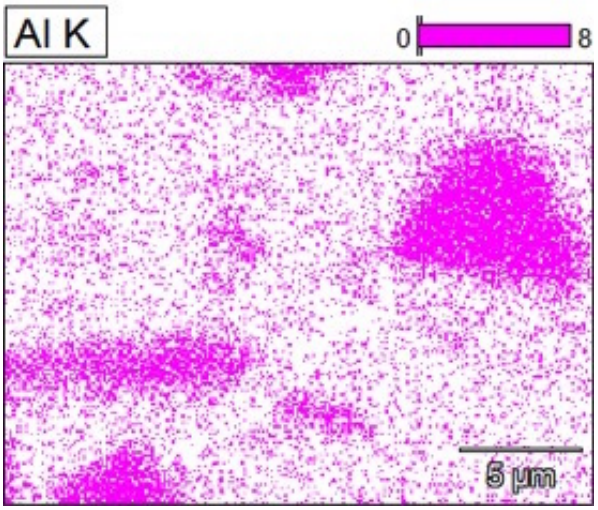

Figure 3.35: EDS results for aluminum on Figure 3.31

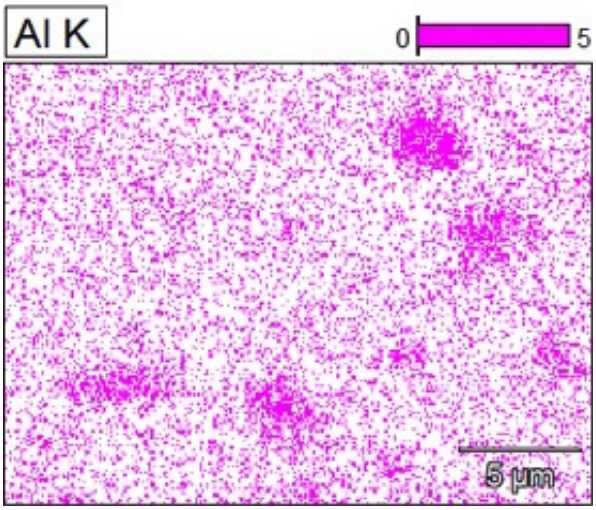

Figure 3.36: EDS results for aluminum on Figure 3.32

As expected, the darker areas have a large concentration of aluminum and an absence of zinc. However, there are both materials in the bulk as well, which indicates that while there was some doping of the bulk, the dopant did prefer to sinter to each other. This might mean that the effect of the doping will not be as ideal as if the dopants were more homogeneously distributed.

3.2.4. ELECTRICAL PROPERTIES

A set of samples were also tested to determine their electrical properties by measuring the resistance at various voltages. All samples, except for the conventionally sintered sample, were gold sputtered. There was some issue with the sputtering where the samples actually turned black, due to believe degassing of the samples. This can be seen in Figure 3.37.

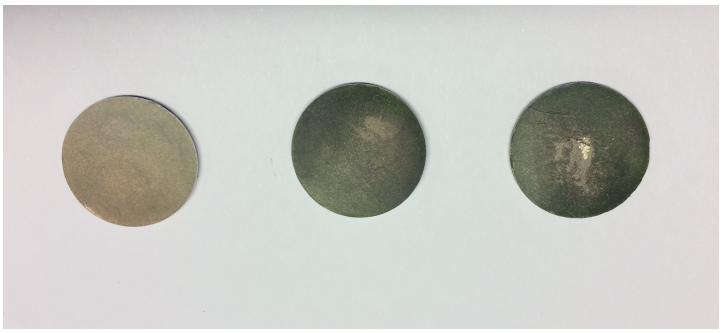

Figure 3.37: 'Gold' sputtered samples

Figure 3.38 shows the overview of all samples. During the testing, each sample reached the overload at different points, which is why not all samples do not progress the exact same range of voltages.

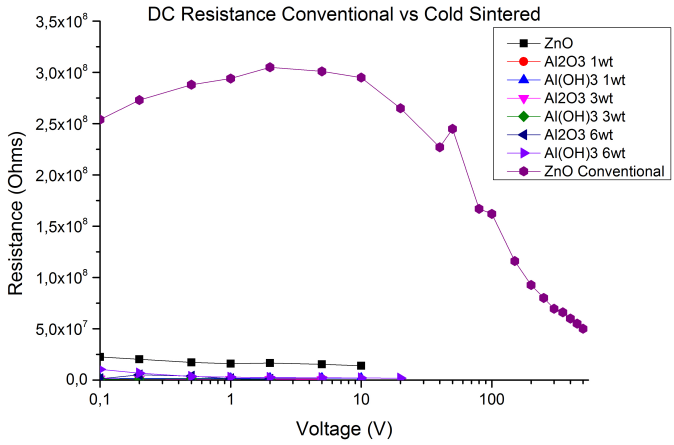

Figure 3.38: Direct current resistance of samples

It is expected that the doping of the samples would increase the conductivity, showing here as a decrease in resistance. First would be that the sample was not gold sputtered due to time constraints. The second could be that the micro-structure is quite different from the cold sintered micro-structure, with larger closely packed grains as well as having a higher density.

Moving to just the cold sintered samples, a close up of that area is shown in Figure 3.39. Again, the pure zinc oxide has a higher resistance.

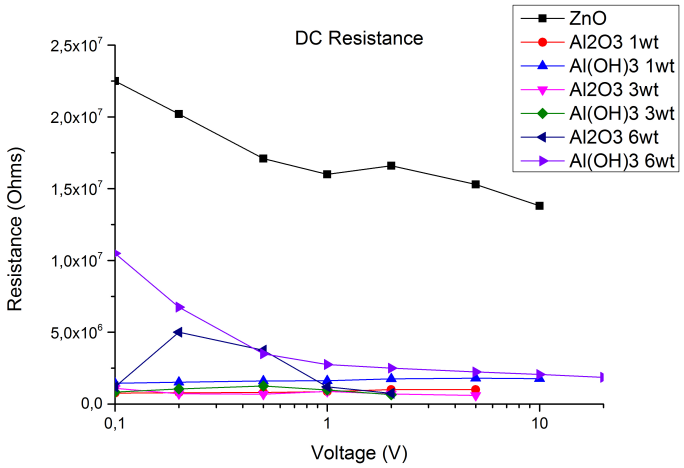

Figure 3.39: Direct current resistance of cold sintered samples

The addition of a dopant has a definite effect on the properties of the material, as in all cases the resistance has decreased, to the same range of resistances. It is expected that adding more dopant will further decrease the resistance of the material. Figure and shows the results broken down into dopant type.

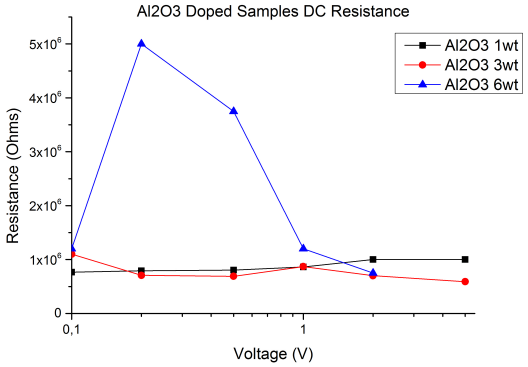

Figure 3.40: Direct current resistance results for aluminum oxide doped samples

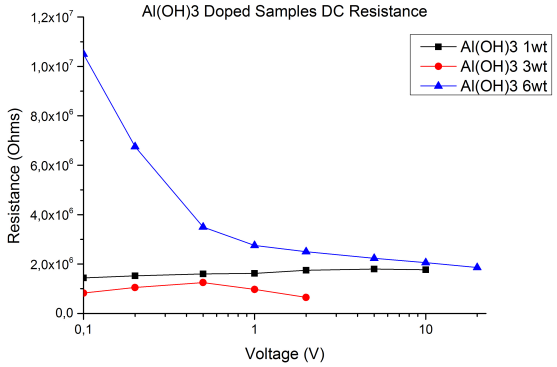

Figure 3.41: Direct current resistance results for aluminum hydroxide hydrate doped samples

As was expected, increasing from the 1 to 3 wt% decreased the resistance of the material, however, this is not the case when the dopant was further increased. In both cases, the 6 wt% samples have a higher resistance than the other doped samples. Even so, the 6 wt% aluminum hydroxide hydrate doped sample had the overall trend which was expected. As was explained earlier in this report, this material should behave as a varistor, meaning that the resistance should decrease as voltage increases. To look at this more in depth, Figure shows the voltage current relationship of the samples calculated using Ohm's law.

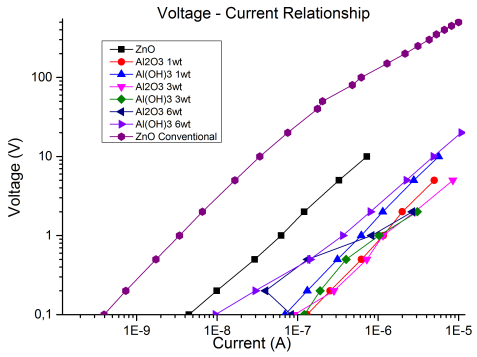

Figure 3.42: Voltage - Current relationship for samples

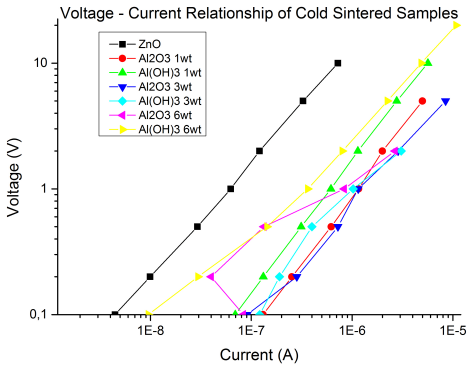

Figure 3.43: Voltage - Current relationship for cold sintered samples

For all of the samples, it appears that they mostly follow the expected trend as was shown in Figure 1.4, where the initial trend in relatively linear until the breakdown point. Since the grain size is so small in the cold sintered samples, it most likely is the case that part of the varying overload is due to this breakdown voltage and the material going from a resistive state to a conductive one. It is not known, however, why the 6 wt% sample has such a different trend compared to the rest of the samples.

3.3. COMPARISON OF PURE AND DOPED MATERIALS

The physical properties of the various pellets differed depending on their composition and manufacturing method. Figure 3.44 shows the various samples.

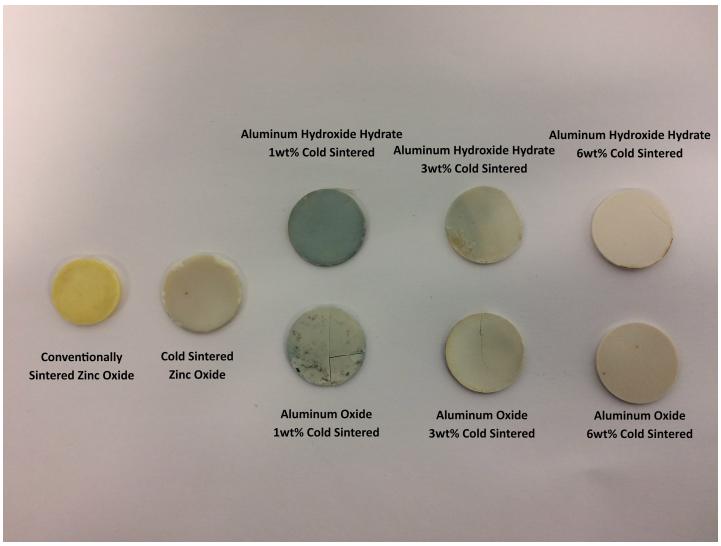

Figure 3.44: Comparison between different samples

The zinc oxide samples were extremely flaky and mostly broke along planes parallel to the pressing plane. The coloring was also not as homogeneous throughout a single ceramic pellet. This made the doped samples much easier to work with compared to the zinc oxide samples, although a lot of resources ended up going into re-making pure samples to have a complete sample for further testing.

In contrast, the doped samples felt very solid and were much more difficult to break, and when they did, they broke on fracture planes perpendicular to the pressing plane. As was shown before, the doped samples have pockets of aluminum rich areas, and the cracking goes around these areas in the material, so it would explain this difference in the material behavior.

When comparing the microstructure to the conventionally sintered samples however, the cold sintered grain size was much smaller. Figure 3.45 shows the conventionally sintered sample's microstructure.

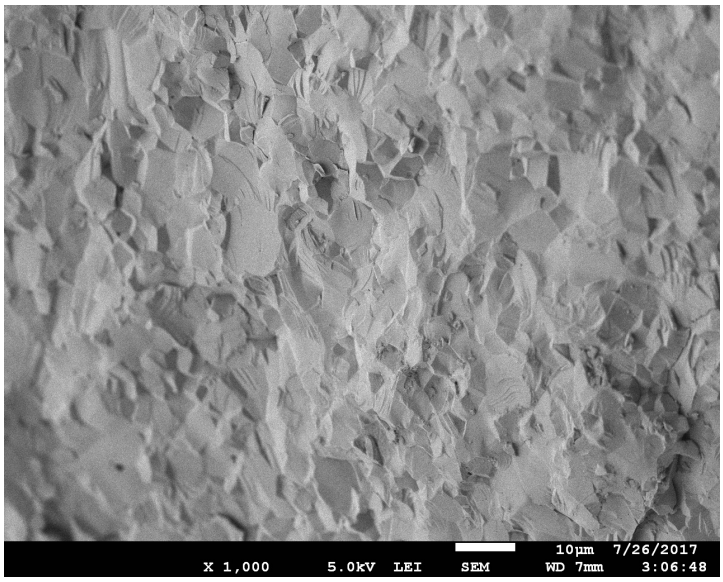

Figure 3.45: Conventionally sintered zinc oxide ceramic

This photo was taken only at 5,000x, however the grains on the fracture plant can be seen clearly in this photo. They are in the range of several μm large, and are all faceted as would be expected. The structure looks very dense as well, with no visible space between the grains as could be seen in images of the samples before. The ideal situation would to have the cold sintered micro-structures look similar to this type of micro-structure.

3.4. SOLVENT PH

In line with the solubility diagrams showed earlier in this report, a short exploration into changing the pH was conducted. Formic acid was used as a replacement acidic solvent, and a solution of ammonia was used as a basic solvent, and deionized water was used as well. The expectation was that the formic acid would successfully create a sample as the solution's pH was lower than what was required based on the solubility diagram for zinc. For the water and ammonia solution, it was expected not to allow for the cold sintering process to progress successfully. This was based on the solubility diagram for zinc, which can be seen in Figure 3.46 with lines marking where the calculated pH of each solvent would approximately be.

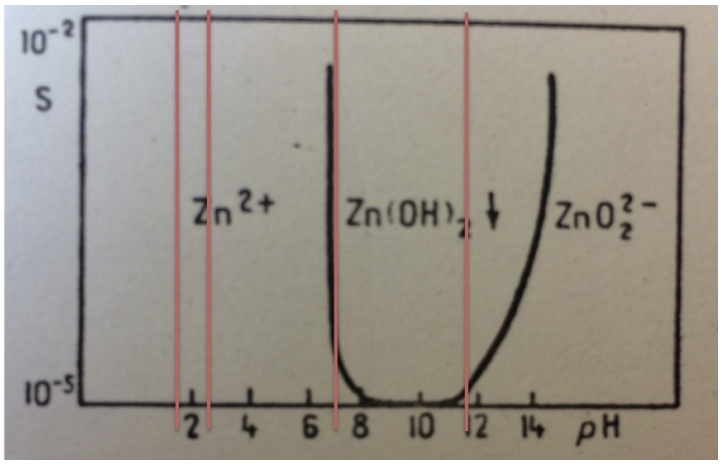

Figure 3.46: Solubility diagram of zinc. Lines going from left to right are: formic acid, acetic acid, water, ammonia [27]

The same parameters were used as was for the doped samples, however only the pure zinc powder was used. Starting with the water and basic solutions, as expected, the resulting pellet was just packed powder after the sintering process, as can be seen in Figures 3.47 and 3.48.

Figure 3.47: Zinc oxide with water as solvent

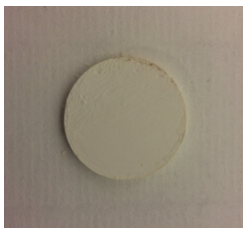

Figure 3.48: Zinc oxide with ammonia as solvent

The coloring of these two samples did not change, staying the powder white color, and broke apart back into a powdery form. In constrast, the sample created with formic acid as the solvent actually became dense, however, with a different texture than the acetic acid samples. Figure 3.50 shows the comparison to the normal acetic acid zinc oxide samples and this new formic acid sample.

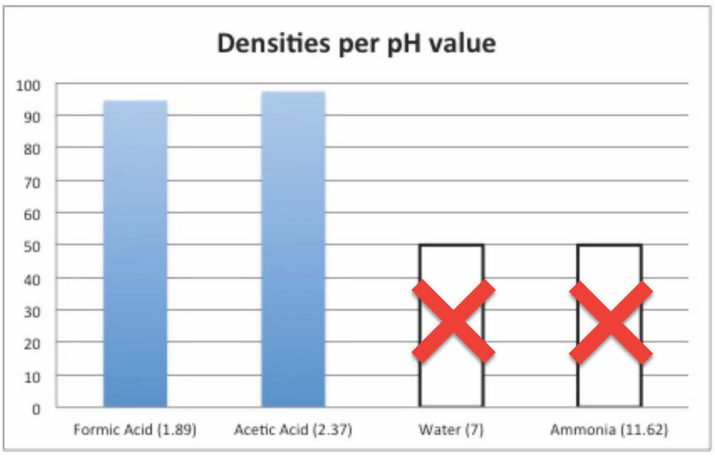

Figure 3.49: Densities versus pH

The outer texture of the formic acid sample was also seemingly more porous compared to the acetic acid samples. This was again seen when the formic acid sample was placed into water for a density measurement. Unlike the acetic acid samples, the formic acid samples released small bubbles for a few minutes on contact with the water. The calculated density of the formic acid sample was 94.5%. A comparison of the densities compared to pH can be seen in Figure .

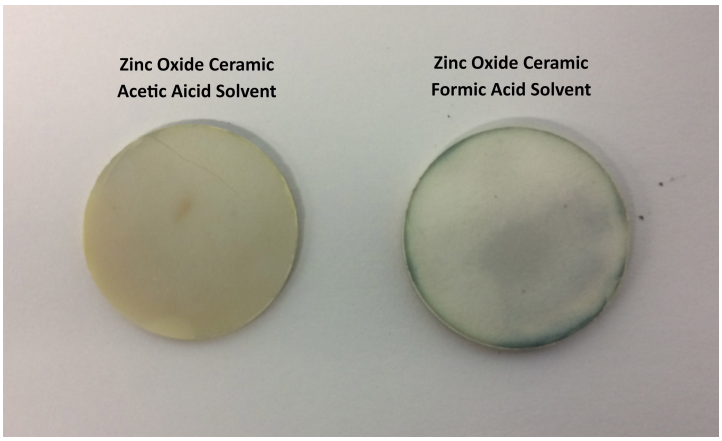

Figure 3.50: Zinc Oxide Ceramics with acetic acid or formic acid

The one downside of using formic acid was that it attacked the mold slightly, leaving some rust in areas after the first use, which can be seen in Figure 3.51.

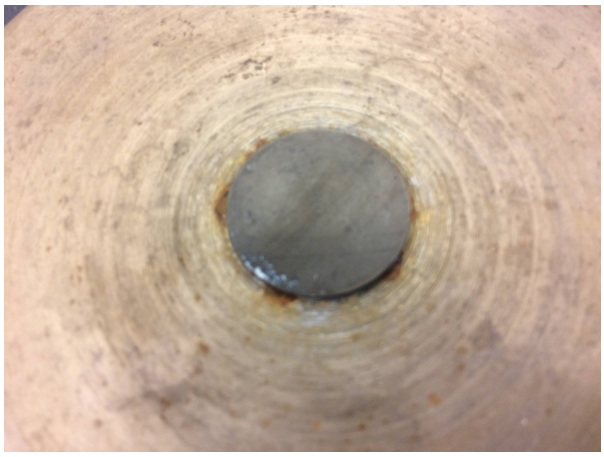

Figure 3.51: Rust formation on steel mold after the formic acid sample was sintered

For the use of acetic acid, rust never formed on the mold just from the cold sintering process. This might be one reason why a slightly less acidic solvent was used for the processing in literature.

Scanning electron images were also taken of the formic acid ceramic microstructure to see if there was any significant difference or change from using a different solvent. Starting at 20,000x magnification, Figure 3.52 shows the microstructure of the material.

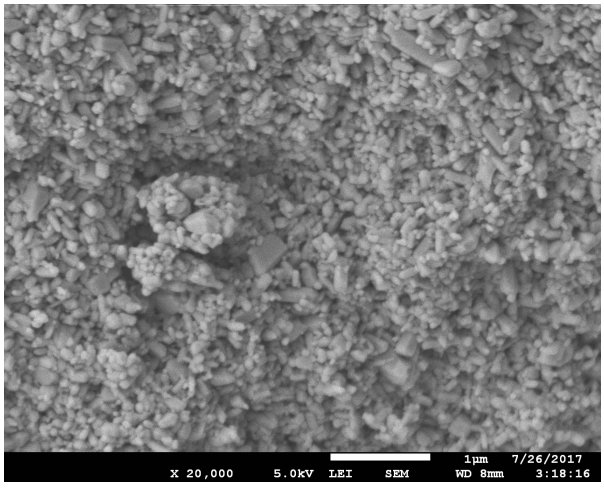

Figure 3.52: Micro-structure of formic acid samples 20,000x

Compared to the acetic acid samples, the grain size is smaller in the formic acid ceramic, and the grains themselves are not very round. This indicates that the sintering process using formic acid might not be as successful as that with acetic acid. Measuring the grains was significantly simpler by using the 50,000x magnification. This closer image can be seen in Figure 3.53.

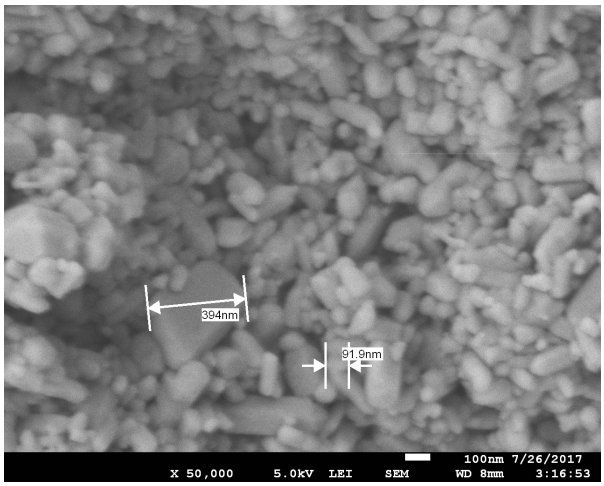

Figure 3.53: Micro-structure of formic acid samples 50,000x

The grainsize of the starting powder was between 40-100 nm, so overall, the grainsize did not improve much compared to this, especially when compared to the acetic acid samples. This further supports the use of acetic acid over other acids, and seems to point to the fact that while the process might work as long as the pH is correct, there is some optimization work within solvent choice which will further assist in the properties of the sintered samples.

3.5. SANDWICH COLD SINTERING

One possible benefit which was explored was the possibility to cold sinter already sintered material. If successful, it would be a new method to be able to join ceramics.

To conduct this experiment, two conventionally sintered and polished samples were required, as well as the normal mold and acetic acid solution. In order to try and limit the cracking of the sintered ceramic under pressure, a layer of powder was put at the bottom of the mold, which can be seen in Figure 3.54.

Figure 3.54: Mold with layer of powder in bottom

This layer of powder should act like a cushion for the samples if the system is not completely flat, especially since only the faces of the ceramic facing each other are polished.

After the powder was placed in the bottom of the mold, one ceramic disk was placed on the powder with the polished surface facing upwards, as shown in Figure 3.55.

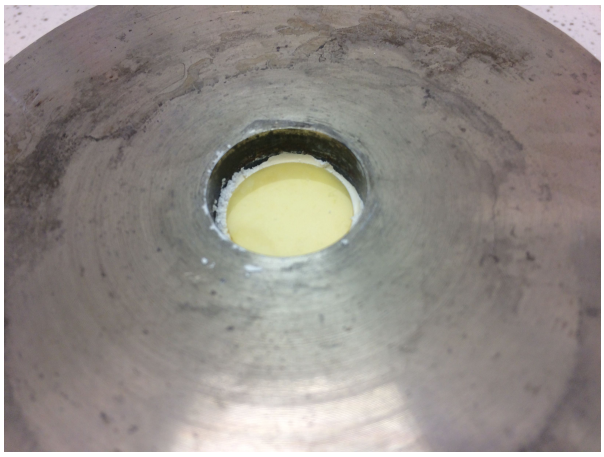

Figure 3.55: Bottom ceramic disk placed in mold

On top of this first disk, one drop of acetic acid was placed, as shown in Figure 3.56. Then the second disk was placed, and another small amount of powder was put on top, as shown in Figure 3.57.

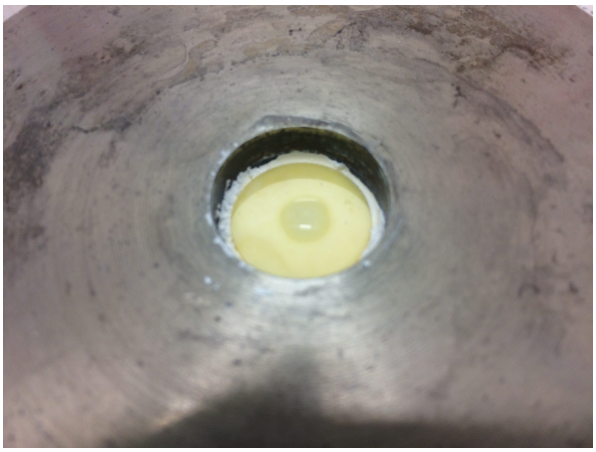

Figure 3.56: Acetic acid droplet on first ceramic plate polished face

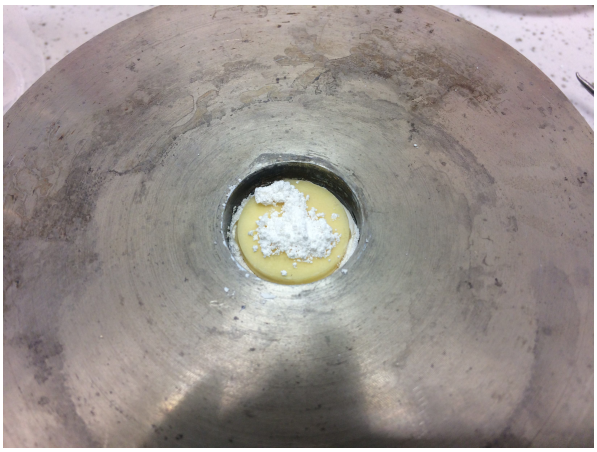

Figure 3.57: Second ceramic plate added and powder placed on top before closure of the mold

From here, the cold sintering process functioned as normal, using the same 150 °C and 15 kN parameters as for the doped samples. After the sintering process, the mold was opened and the paper disk and lower ceramic plate were visible, as shown in Figure 3.58.

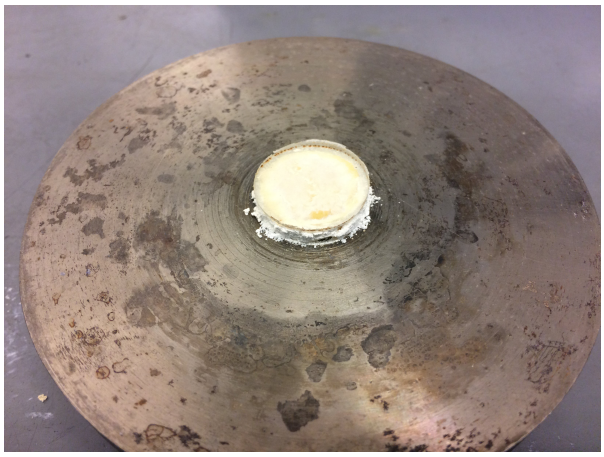

Figure 3.58: Sample after cold sintering process

The paper was then removed from the sample, and unfortunately, the lower ceramic plate came with it. As Figure 3.59 shows, there was no visible change to the ceramic.

Figure 3.59: Sample after cold sintering process

From this, a portion of the touching face was analyzed under the scanning electron microscope to determine if there was any visible changes to the surface. Figure 3.60 shows the overview of the sample.

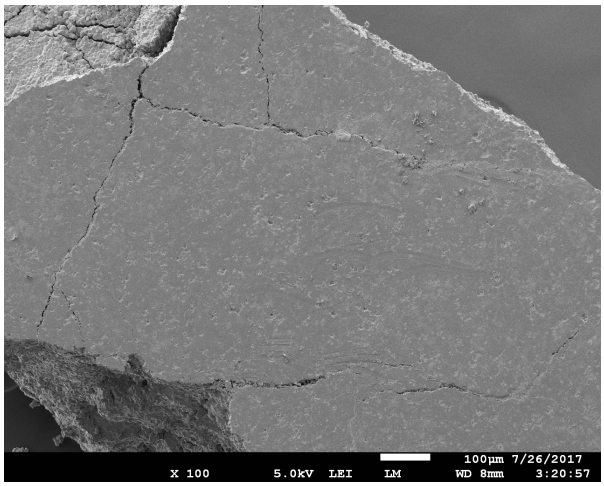

Figure 3.60: Sintered face x100

The overall face is quite smooth, with some pockets within the surface. This could indicate that the grain size was too large for the acid to actually effectively dissolve the grains. Taking a closer look, Figure 3.61 and 3.62 show these pockets within the material.

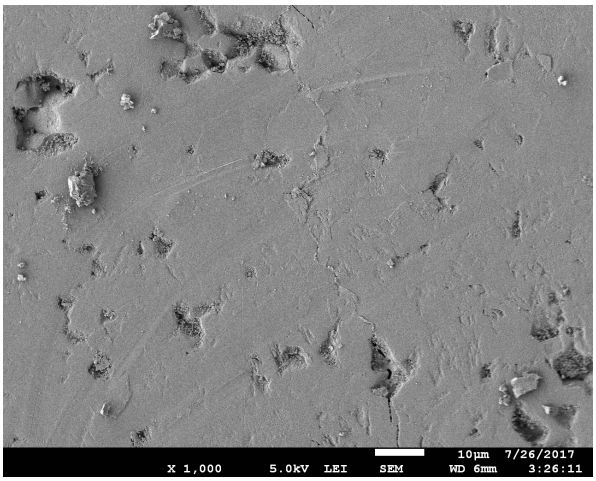

Figure 3.61: Sintered face x1000

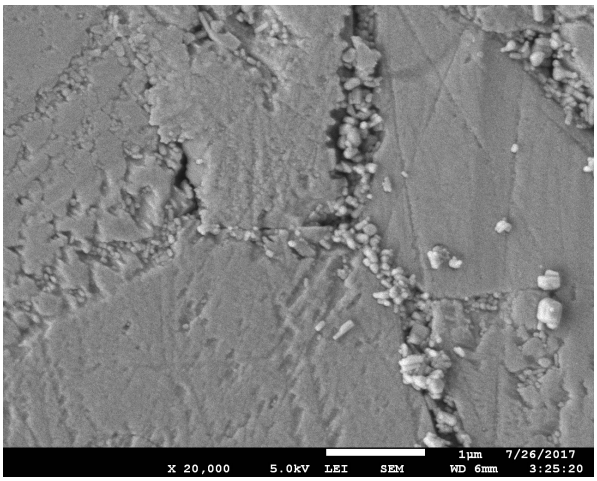

Figure 3.62: Sintered face x20,000

The valleys within the material are not particularly deep nor are they widespread over the surface. However, when looking more closely, it seems as though there are grains within these valleys. This could be from two different sources; the particles could be from the actual acid and sintering process, or it could be contamination from the powder used to protect the samples during sintering. Either way, this type of sintering does not seem to be effective. Further work could be done to see if leaving the acid on the samples for a longer time before sintering would help in the process. As well, since the pellets themselves cracked into many pieces during the process, a different method of cold sintering could also be explored to prevent this.

3.6. ANNEALING

After cold sintering, a set of ceramic pellets, one made of zinc oxide, one doped with 6 wt% aluminum hydroxide hydrate, and one doped with 6 wt% aluminum oxide were put

through a set of heat treatments to determine if they would have an effect on the density of the material. The samples were photographed, density measured using Archimedes method, and then placed into the furnace. The heating rate used was 5 °C per minute, and the hold time at the specific temperature was 1 hour.

The temperatures which were used was 300, 400, 500, 600, 700, 800, 900, and 1000 °C, with measurements and photos taken between each step.

It was found that the density increased starting with the first step, particularly for the doped samples. Figure 3.63 shows this increase in density with the temperature steps.

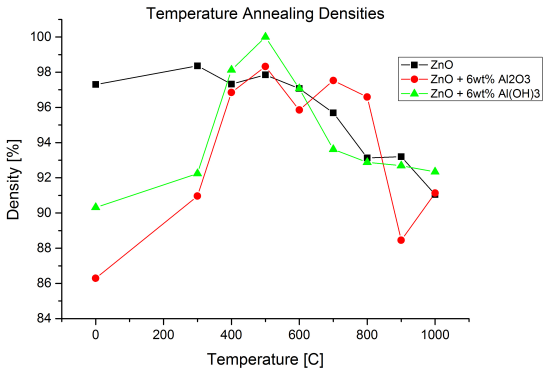

Figure 3.63: Densities of ceramics at each temperature step

For the two doped samples, there was quite some air bubbles which would escape during the water immersion step of the density measurements. This was particularly seen with the aluminum oxide samples, and for the post 500 °C measurement, the stabilizing of the immersed weight took some minutes. This bubbling of the samples corresponds to the peak of the density graph, and with higher temperatures, the bubbling decreased, along with the density. What this seems to indicate, especially when taking into account the electrical measurements, is that there is some sort of liquid or glassy phase which is present after the cold sintering process, and once the temperature is raised enough, this phase disappears. This can also be seen somewhat through the color change as well.

For the color change, the samples progressively got darker from their white starting color, shown in Figure 3.64.

Figure 3.64: Samples taken before the first temperature step. Left to right: Zinc Oxide, 6 wt% aluminum oxide doped, 6 wt% aluminum hydroxide hydrate doped

All three samples in the beginning are quite white, with the doped samples being slightly darker. This is in contrast to the conventionally sintered samples shown eariler, which were

bright yellow. However, when adding the temperature treatment, the samples do start to get darker, shown in Figure 3.65.

Figure 3.65: Samples taken after 300 °C. Left to right: Zinc Oxide, 6 wt% aluminum oxide doped, 6 wt% aluminum hydroxide hydrate doped

After being heated for an hour at 300 °C, the samples were noticeably darker than before, with the zinc oxide sample now being the darkest sample with a grey color. The other two samples also darkened, but not as much. Figure 3.66 shows the samples after 400 °C, where the color changes further.

Figure 3.66: Samples taken after 400 °C. Left to right: Zinc Oxide, 6 wt% aluminum oxide doped, 6 wt% aluminum hydroxide hydrate doped

As can be seen, the samples actually get a bit lighter after this temperature step. The bottom of the zinc oxide sample has a tint of yellow, and the other two samples are also moving to a yellow color. When heating the samples to 500 °C, this trend seems to continue, as can be seen in Figure 3.67.

Figure 3.67: Samples taken after 500 °C. Left to right: Zinc Oxide, 6 wt% aluminum oxide doped, 6 wt% aluminum hydroxide hydrate doped

The yellow area on the bottom of the zinc oxide sample has started to move upwards, covering now more than half of the surface of the sample, with the rest being grey. The

other two doped samples are turning more yellow/white. Figure 3.68 shows the samples after 600 °.

Figure 3.68: Samples taken after 600 °C. Left to right: Zinc Oxide, 6 wt% aluminum oxide doped, 6 wt% aluminum hydroxide hydrate doped

After this temperature step of 600 °C, the samples are slightly brighter/yellower, but the overall trend of patterning on the zinc oxide sample continues with the upper part being grey still and the rest yellow. However, this grey area has gotten smaller. Figure 3.69 shows the samples after 700 °C, where the complete samples are now a single color, the zinc oxide a very pale yellow, and the doped samples closer to white.

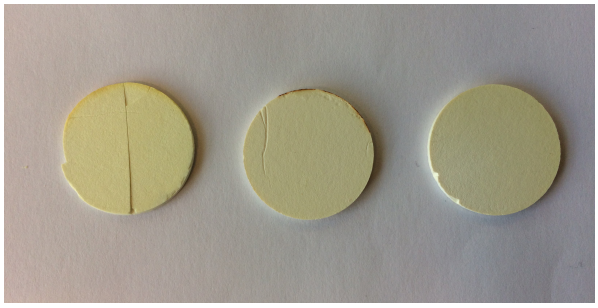

Figure 3.69: Samples taken after 700 °C. Left to right: Zinc Oxide, 6 wt% aluminum oxide doped, 6 wt% aluminum hydroxide hydrate doped

This trend continues with the higher temperature, with the samples staying this pale color. Figure 3.70 shows the samples after 800 °C.

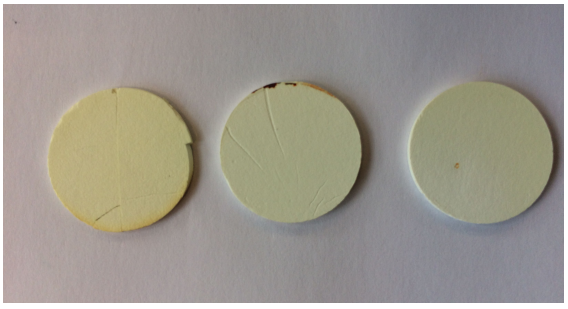

Figure 3.70: Samples taken after 800 °C. Left to right: Zinc Oxide, 6 wt% aluminum oxide doped, 6 wt% aluminum hydroxide hydrate doped

Even though the density is still decreasing with these higher temperatures, the material

stays the same color. Figure 3.71, showing the samples after 900 °C, has the same coloring as the previous temperature step.

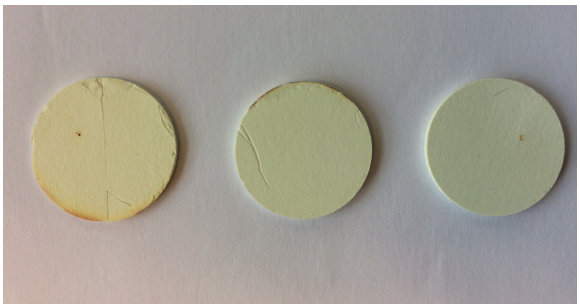

Figure 3.71: Samples taken after 900 °C. Left to right: Zinc Oxide, 6 wt% aluminum oxide doped, 6 wt% aluminum hydroxide hydrate doped

The final step of this test was 1000 °C, 100 degrees below the temperature used for the conventional sintering. However, as seen in Figure 3.72, these pre-cold sintered samples do not obtain that yellow coloring after being heated to this temperature.

Figure 3.72: Samples taken after 1000 °C. Left to right: Zinc Oxide, 6 wt% aluminum oxide doped, 6 wt% aluminum hydroxide hydrate doped

It seems as though there is another unexpected phase within the cold sintered material which could explain the electrical results showing the material to be a conductor instead of an insulator. It seems as though this phase might burn out around 500 °C, corresponding to the material turning from grey to more of a pale yellow color. Bubbling was seen during the density test around this temperature as well, demonstrating that the structure did have some gaps. The densitites now also represent densities close to those measured using the volume of the sample, in the low 90's to high 80's.

In order to determine if there was another phase or some sort of microstructure phase, the annealed samples then were tested and new diffraction patterns taken and compared to the original samples' patterns. Figure 3.73 shows the three new patterns taken.

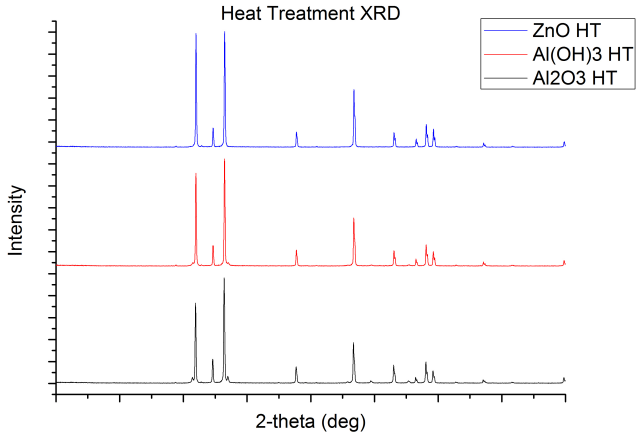

Figure 3.73: XRD diffraction patterns taken after heat treatment for zinc oxide (ZnO), aluminum hydroxide hydrate ($Al(OH)_3$), and aluminum oxide (Al_2O_3) doped samples

From this, it can be seen that there is a difference between the three diffraction patterns. The pure zinc oxide samples has very sharp peaks compared to the other two diffraction patterns, where there appear to be shoulders on the sides of the larger peaks. Comparing these to the diffraction patterns taken before Figure 3.74 shows the comparison between the two zinc oxide diffraction patterns.

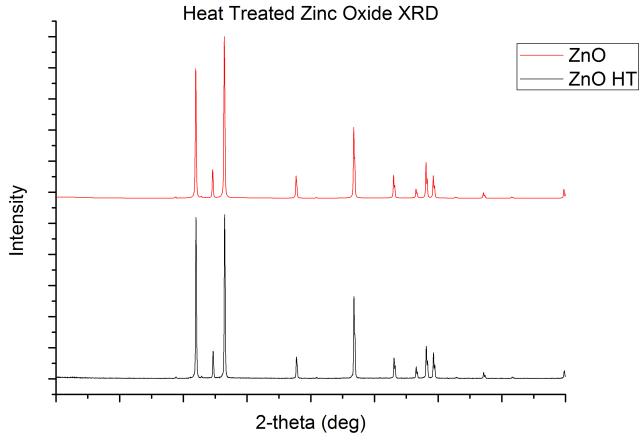

Figure 3.74: XRD diffraction patterns taken after heat treatment for zinc oxide (ZnO)

For the pure zinc oxide sample, there does not seem to be any difference shown after the annealing process. This might explain the fact that the original density was already quite high and showed little improvement compared to the doped samples. Moving to the doped samples,

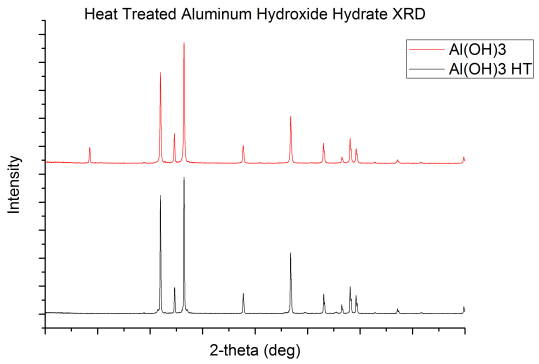

Figure 3.75: Aluminum hydroxide hydrate ($Al(OH)_3$) doped samples before and after heat treatment (HT)

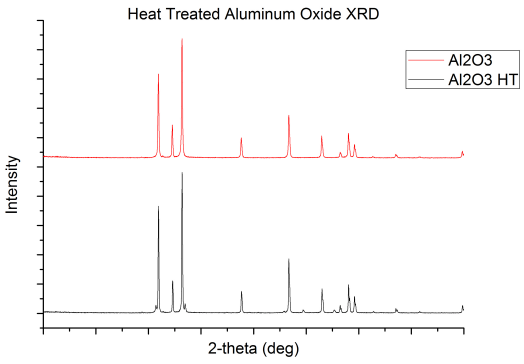

Figure 3.76: Aluminum oxide (Al_2O_3) doped samples before and after heat treatment (HT)

There are some slight changes in these diffraction patterns. For the aluminum hydroxide hydate doped sample, the lowest peak has disappeared, and the aluminum oxide doped sample gains some shoulders around the larger peaks. Comparing these to the library measurements, Figure shows the diffraction pattern of the aluminum hydroxide hydrate sample compared to the library patterns.

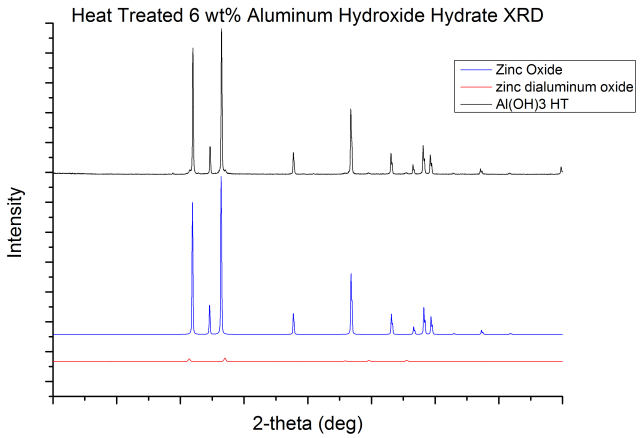

Figure 3.77: Aluminum hydroxide hydrate ($Al(OH)_3$) diffraction pattern compared to the library patterns

In the heat treated sample, there is a different appearance of aluminum. In this case, there is zinc dialuminum oxide, instead of the Gibbsite, or aluminum hydroxide. For the aluminum oxide doped sample, Figure 3.78 shows the comparison of the diffraction patterns.

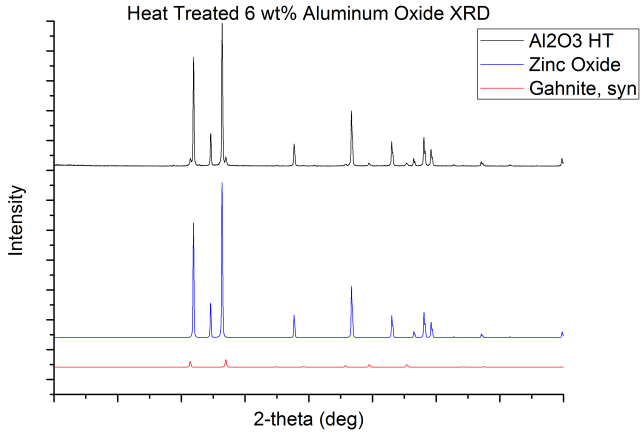

Figure 3.78: Aluminum oxide (Al_2O_3) diffraction pattern compared to the library patterns

After the heat treatment, the aluminum shows up in Gahnite form, which is $ZnAl_2O_4$. Before the heat treatment aluminum appeared in the aluminum oxide form. It seems that the heat treatment or annealing allows for the dopant to better diperse within the material, going from the same format as their powder form, to a more integrated format within the material. Perhaps this shift could explain some of the density changes within the material as well as the color change seen during the heat treatment process.

4

Conclusion

The main objective of this thesis was to determine if cold sintering zinc oxide ceramics could be reproduced, and if so, what parameters work the best to have high density ceramics. As this process has very little scientific literature, a successful reproduction would be required in order to progress to the following stages. Once this process was successfully developed, an exploration into the pH of the solvent, doping of the powders, and their effects on the process were the next steps. Analysis of the micro-structure as well as the electrical properties, and color were used.

In conclusion, it was proven that it is possible to sinter zinc oxide ceramics. While the final properties were not the ideal, there was visible grain growth and densification. Using the density measurements, a set of parameters were chosen to then determine if using the bulk properties of the material were enough to allow cold sintering of a doped material. Lower pressures were found to allow for better grain growth, with an optimum at 15 kN. These parameters take into account the solubility diagrams of all components of the material, making sure that all grains are soluble in the solvent being used.

Using the solubility diagrams for zinc, the pH aspect of the solvent was explored. It was found that the process will not function if the pH was in the precipitation part of the phase, for most materials in the neutral area and surroundings. A slightly stronger acid was used as a trial, and while the process still worked in agreement with the solublity diagrams, the micro-structure of the material was different, with smaller grains.

This doped system was also found to also successfully work, however, as the dopant amount increased in the system, the density decreased, pointing to a possibility that as the system changes, the sintering parameters also might need to change. These doped samples were also less brittle. As well, when analyzing the polished fracture face, it was found that the dopants were not completely homogeneously mixed throughout the ceramic, and that there were dopant rich areas.

When heat treating the samples after cold sintering, this low density increased already at relatively low temperatures, around 300 °C. This increase in density however, declines again starting at 600 °C, perhaps indicating that another phase is present in the material.

The doped structure appears to be conductive in nature, presenting itself in the direct current resistance measurements. As expected, the adding of the dopant decreased the resistance of the material, meaning that the doping of the pure zinc oxide was successful. However, increasing the amount of dopant did not continue this trend, with the resistance of the 6 wt% doped material was higher than the other doped materials for both dopant types.

4.1. RECOMMENDATIONS

There are number of recommendations for future research based on this project. Starting at the beginning of the cold sintering process, since the solvent appears to be the backbone of the process, an analysis of the solvent choice compared to the final grain parameters would be a prudent start. Further down the process, a more in depth analysis of the parameters, especially to assist in the brittleness of the final samples would be needed.

For the doped samples, an analysis into changing the parameters to achieve high densities with the higher wt% samples would be a start. One possibility would be to look at aluminum oxide ceramics, and to determine if perhaps the parameters to cold sinter this ceramic would be similar to a better optimum for these doped ceramics.

It might be the case that part of the issue encountered with the small final grain size was partially due to the chosen powders. Based on the literature, a small grain size was recommended, however, it might be the case that the powders used for this were too small.

The density decrease during the temperature annealing should be explored. If taken into account with the issues with the gold sputtering, it might be that there is another unexpected phase within the material. Further research should be conducted to determine if this is the case.

BIBLIOGRAPHY

[1] S. Rana and J. Fangueiro, R. Silva, Nunes, *Advanced Composite Materials for Aerospace Engineering*, Vol. 2023 (Elsevier Ltd, 2016) pp. 1–15, 129–174.

[2] E. De Guire, *Ceramic Engineering in Aerospace,* The American Ceramic Society (2013).

[3] Rolls-Royce, *The jet engine,* (1996), arXiv:0902121049 .

[4] J. Guo, H. Guo, A. L. Baker, M. T. Lanagan, E. R. Kupp, G. L. Messing, and C. A. Randall, *Cold Sintering: A Paradigm Shift for Processing and Integration of Ceramics,* Angewandte Chemie - International Edition **16802**, 11457 (2016).

[5] E. De Guire, *History of Ceramics | The American Ceramic Society,* (2014).

[6] E. Monfort, A. Mezquita, and E. Vaquer, *8.05 – Ceramic Manufacturing Processes: Energy, Environmental, and Occupational Health Issues,* Comprehensive Materials Processing , 71 (2014).

[7] J. Holterman and P. Groen, *An Introduction to Piezoelectric Materials and Applications*, ii ed. (Stichtung Applied Piezo, Apeldoorn, 2013).

[8] W. D. Kingery, H. K. Bowen, and D. R. Uhlmann, *Introduction to ceramics*, 2nd ed., Wiley series on the science and technology of materials (Wiley, 1976).

[9] C. F. Klingshirn, B. K. Meyer, A. Waag, A. Hoffmann, and J. Geurts, *Springer Series in Materials Science*, 1 (Springer, 2010) p. 366.

[10] K. Ellmer, A. Klein, and B. Rech, *Transparent Conductive Zin Oxide Basic and Applications in Thin Film Solar Cells* (2008) p. 453.

[11] K. Byrappa and Masahiro Yoshimura, *Handbook of Hydrothermal Technology*, 2nd ed. (Elsevier Inc., 2013) arXiv:arXiv:1011.1669v3 .

[12] AAB, *Technical information - Physical properties of zinc oxide varistors*, Tech. Rep. (AAB Power Technology Products AB, 2002).

[13] A. Moulson and J. Herbert, *Electroceramics - Materials, Properties, Ceramics* (Chapman & Hall, London, 1995).

[14] Y. M. Chiang, D. P. Birnie, and W. D. Kingery, *Physical Ceramics: Principles for Ceramic Science and Engineering* (Wiley, 1996).

[15] H. Morkoç and Ü. Özgür, *Zinc Oxide: Fundamentals, Materials and Device Technology* (Wiley-VCH, Weinheim, Germany, 2009) pp. 1–477.

[16] W. Zhong Lin, *Zinc oxide nanostructures: growth, properties and applications,* Journal of Physics: Condensed Matter **16**, R829 (2004).

[17] H.-H. Bechtel, Y. Martynov, W. Busselt, W. A. Groen, and P. Huppertz, *Display Device with Varistor Layer,* (2004).

[18] M. Rahaman, *Ceramic Processing and Sintering*, 1st ed. (Marcel Dekker Inc., New York, 1995).

[19] H. Guo, A. Baker, J. Guo, C. A. Randall, and D. Johnson, *Cold Sintering Process: A Novel Technique for Low-Temperature Ceramic Processing of Ferroelectrics,* Journal of the American Ceramic Society **99**, 3489 (2016).

[20] H. Guo, A. Baker, J. Guo, and C. A. Randall, *Protocol for Ultralow-Temperature Ceramic Sintering: An Integration of Nanotechnology and the Cold Sintering Process,* ACS Nano , acsnano.6b03800 (2016).

[21] L. Zhang, Y. Ben, H. Chen, D. Tang, X. Fu, R. Sun, B. Song, and C. Wong, *Low temperature-sintering and microstructure of highly transparent yttria ceramics,* Journal of Alloys and Compounds **695**, 2580 (2017).

[22] R. M. German, P. Suri, and S. J. Park, *Review: Liquid phase sintering,* Journal of Materials Science **44**, 1 (2009).

[23] R. T. P. P. A. de Vries, ed., *Ceramic Processing*, 1st ed. (Chapman & Hall, London, 1995).

[24] S.-J. L. Kang, *5 - Liquid phase sintering,* in *Sintering of Advanced Materials - Fundamentals and Processes*, edited by Z. Z. Fang (Woodhead Publishing, 2010) pp. 110–129.

[25] R. German, *Liquid Phase Sintering*, 1st ed. (Plenum Press, New York, 1985).

[26] A. Kopp, A. Carlos, P. Bergmann, and F. Amorim Berutti, *Novel Synthesis and Characterization of Nanostructured Materials* (2013) pp. 1–85.

[27] G. Charlot, *L'Analyse Qualitative et les Réactions en Solution* (Masson et Cie, Paris, 1963).

[28] AZoM, *Cold Sintering Process Helps Develop New Materials and Reduce Energy Cost,* , 2 (2016).

[29] H. Kähäri, M. Teirikangas, J. Juuti, and H. Jantunen, *Improvements and modifications to room-temperature fabrication method for dielectric Li2MoO4 ceramics,* Journal of the American Ceramic Society **98**, 687 (2015).

[30] H. Kähäri, M. Teirikangas, J. Juuti, and H. Jantunen, *Room-temperature fabrication of microwave dielectric Li2MoO4-TiO2 composite ceramics,* Ceramics International **42**, 11442 (2016).

[31] H. Guo, J. Guo, A. Baker, and C. A. Randall, *Hydrothermal-Assisted Cold Sintering Process: A New Guidance for Low-Temperature Ceramic Sintering,* ACS Applied Materials and Interfaces **8**, 20909 (2016).

[32] S. Funahashi, J. Guo, H. Guo, K. Wang, A. L. Baker, K. Shiratsuyu, and C. A. Randall, *Demonstration of the Cold Sintering Process Study for the Densification and Grain Growth of ZnO Ceramics,* Journal of the American Ceramic Society **6**, 1 (2016).

[33] H. Guo, T. J. M. Bayer, J. Guo, A. Baker, and C. A. Randall, *Scripta Materialia Current progress and perspectives of applying cold sintering process to ZrO 2 -based ceramics,* (2017), 10.1016/j.scriptamat.2017.02.004.

[34] J. Guo, A. L. Baker, H. Guo, M. Lanagan, and C. A. Randall, *Cold Sintering Process: A New Era for Ceramic Packaging and Microwave Device Development,* Journal of the American Ceramic Society **7**, 1 (2016).

[35] J. Guo, S. S. Berbano, H. Guo, A. L. Baker, M. T. Lanagan, and C. A. Randall, *Cold Sintering Process of Composites: Bridging the Processing Temperature Gap of Ceramic and Polymer Materials,* Advanced Functional Materials **26**, 7115 (2016).

[36] H. Guo, J. Guo, A. Baker, and C. A. Randall, *Cold Sintering Process for ZrO 2 -Based Ceramics: Significantly Enhanced Densification Evolution in Yttria-Doped ZrO 2,* Rapid Communication **4**, 1 (2016).

[37] T. K. Roy, D. Bhowmick, D. Sanyal, and A. Chakrabarti, *Sintering studies of nanocrystalline zinc oxide,* Ceramics International **34**, 81 (2008).

[38] M. Mazaheri, *Sintering of Nanocrystalline Zinc Oxide via Conventional Sintering , Two Step Sintering and Hot Pressing,* , 1 (2009).